JEM Journal of Experimental Medicine

ARTICLE

TIPE2 specifies the functional polarization of myeloid-derived suppressor cells during tumorigenesis

Dehong Yan[1], Jinghui Wang[1,2], Honghong Sun[3], Ali Zamani[3], Honglin Zhang[1], Weihong Chen[4], Aifa Tang[4], Qingguo Ruan[1], Xiaolu Yang[5], Youhai H. Chen[3], and Xiaochun Wan[1]

Myeloid-derived suppressor cells (MDSCs) are "polarized" myeloid cells that effectively promote tumorigenesis by inhibiting antitumor immunity. How myeloid cells acquire the protumoral properties during tumorigenesis is poorly understood. We report here that the polarity protein TIPE2 (tumor necrosis factor-α–induced protein 8-like 2) mediates the functional polarization of murine and human MDSCs by specifying their pro- and antitumoral properties. Tumor cells induced the expression of TIPE2 in Gr1$^+$CD11b$^+$ cells through reactive oxygen species (ROS). TIPE2 in turn increased the expression of protumoral mediators such as CCAAT/enhancer-binding protein-β while inhibiting the expression of antitumoral mediators. Consequently, tumor growth in TIPE2-deficient mice was significantly diminished, and TIPE2-deficient MDSCs markedly inhibited tumor growth upon adoptive transfer. Pharmaceutical blockade of ROS inhibited TIPE2 expression in MDSCs and reduced tumor growth in mice. These findings indicate that TIPE2 plays a key role in the functional polarization of MDSCs and represents a new therapeutic target for cancer immunotherapy.

Introduction

Myeloid-derived suppressor cells (MDSCs) are a heterogeneous subpopulation of leukocytes important for cancer and inflammatory diseases (Bronte et al., 2016; He et al., 2018; Kumar et al., 2016b; Manjili, 2012; Solito et al., 2012; Trikha and Carson, 2014; Zhou et al., 2018). Although MDSCs are present in low numbers in healthy individuals, they increase markedly in patients with cancer or chronic inflammation (comprising ≤10% of leukocytes in the blood or spleen; Bronte et al., 2016; Gabrilovich, 2017; Kumar et al., 2016b; Manjili, 2012; Solito et al., 2012; Trikha and Carson, 2014; Zhou et al., 2018). This increase results from aberrant myelopoiesis driven by inflammatory mediators. MDSCs, but not monocytes or neutrophils, are potent suppressors of immune responses (Kumar et al., 2016b; Manjili, 2012; Solito et al., 2012; Trikha and Carson, 2014; Zhou et al., 2018). Depletion of MDSCs leads to markedly enhanced antitumor immunity and may be crucial for the success of cancer immunotherapy (Srivastava et al., 2012; Stromnes et al., 2014; Veglia et al., 2018, 2019). Phenotypically, MDSCs are similar to monocytes and neutrophils, but functionally and biochemically they are distinct from the latter cell subsets. MDSCs are "polarized" immature myeloid cells, producing selectively inhibitory but not inflammatory mediators of myeloid cells (Bronte et al., 2016; Gabrilovich, 2017; Kumar et al., 2016b; Manjili, 2012; Solito et al., 2012; Trikha and Carson, 2014; Zhou et al., 2018). In mice, MDSCs are defined as cells expressing both Gr1 and CD11b markers, which can be further divided into two subpopulations: granulocytic (G)-MDSCs (CD11b$^+$Ly6G$^+$Ly6C^{low}) and monocytic (M)-MDSCs (CD11b$^+$Ly6G$^-$Ly6C^{high}). In humans, G-MDSCs are defined as CD11b$^+$CD14$^-$CD15$^+$ or HLA-DR$^{-/low}$CD33$^+$CD14$^{-/low}$CD66b$^+$, and M-MDSCs as CD11b$^+$CD14$^+$HLA-DR$^{-/low}$CD15$^-$ or HLA-DR$^{-/low}$CD33$^+$CD14$^+$CD66b$^-$ (Veglia et al., 2018; Yan et al., 2019). Despite their significance in cancer and inflammatory diseases, MDSCs remain one of the least understood subsets of leukocytes. It is unclear what specifies the polarized differentiation program of MDSCs, and it is unknown how the inflammatory property of the myeloid lineage is held in check in MDSCs.

MDSC development is driven by at least two transcription factors: CCAAT/enhancer-binding protein-β (C/EBPβ) and STAT3 (Cheng et al., 2008; Condamine et al., 2015; Hirai et al., 2006;

[1]Shenzhen Laboratory for Human Antibody Engineering, Center for Protein and Cell-based Drugs, Shenzhen Institutes of Advanced Technology, Chinese Academy of Sciences, Shenzhen, China; [2]College of Life Science and Technology, Jinan University, Guangzhou, China; [3]Department of Pathology and Laboratory Medicine, Perelman School of Medicine, University of Pennsylvania, Philadelphia, PA; [4]Department of Hematology, The First Affiliated Hospital of Shenzhen University, Shenzhen Second People's Hospital, Shenzhen, China; [5]Abramson Family Cancer Research Institute, Perelman School of Medicine, University of Pennsylvania, Philadelphia, PA.

Correspondence to Youhai H. Chen: yhc@pennmedicine.upenn.edu; Xiaochun Wan: xc.wan@siat.ac.cn.

Kumar et al., 2016a; Marigo et al., 2010; Mildner et al., 2017; Ostrand-Rosenberg, 2010; Tamura et al., 2017). C/EBPβ (also known as NF-IL6) contains an N-terminal transcriptional activation domain, a C-terminal DNA binding domain, and a pair of central regulatory domains (RDs; Maekawa et al., 2015). RD2 is a Ser/Thr-rich region with multiple potential phosphorylation sites (Li et al., 2008; Shen et al., 2009). Phosphorylation of Thr188 mediated by ERK and phosphorylation of Thr179 mediated by glycogen synthase kinase 3β (GSK-3β) inhibit the ability of C/EBPβ-RD2 to bind to DNA. There are at least three isoforms of C/EBPβ: liver-enriched activator proteins (LAP* and LAP), which function as major transcriptional activators of inflammation-related genes such as IL-6, IL-10, and ARG1 (Li et al., 2008; Ruffell et al., 2009), and liver-enriched inhibitory protein (LIP), which lacks the DNA transactivation domain and reduces inflammation by blocking LAP and LAP* activity (Park et al., 2013; Rehm et al., 2014). STAT3 is activated by cytokines such as IL-6, IL-10, and vascular endothelial growth factor (Cheng et al., 2008; Kumar et al., 2016b). IL-6 plays a critical role in the induction of phosphorylation of STAT3, which directly induces the expression of ARG1 and inducible nitric oxide synthase (iNOS) and the production of ROS in the nucleus (Gabrilovich, 2017; Marigo et al., 2008). C/EBPβ can regulate STAT3 activity by controlling IL-6 levels in MDSCs. Conversely, STAT3 can also directly regulate C/EBPβ activity (Lee et al., 2002; Panopoulos et al., 2006; Zhang et al., 2010a). In the chronic inflammatory hypoxic environment, STAT3 and C/EBPβ activity can be regulated by microRNA-142-3p, which targets the IL-6 receptor gp130 (also called CD130) on MDSCs (Kumar et al., 2016a; Sonda et al., 2013). Therefore, C/EBPβ and STAT3 regulation in MDSCs is complex and remains to be fully characterized.

TIPE2 (tumor necrosis factor-α–induced protein 8-like 2, or TNFAIP8L2), is a member of the TIPE family that is preferentially expressed by leukocytes (Sun et al., 2008; Zhang et al., 2009). TIPE2 is a "professional" transfer protein of phosphoinositide second messengers (Fayngerts et al., 2017). It controls leukocyte polarity during migration by acting as both a local enhancer and a global inhibitor of signal transduction (Fayngerts et al., 2017). TIPE2 is also an essential regulator of inflammation and immune homeostasis (Sun et al., 2008; Suo et al., 2016). Overexpression of TIPE2 in tumor cells can induce cell death and significantly inhibit Ras-induced tumorigenesis in mice (Gus-Brautbar et al., 2012). TIPE2 regulates cell death by binding to the Ras-interacting domain of RGL (Ral GDP dissociation stimulator-like) and inhibiting the activation of the downstream signaling molecules Ral and AKT (Gus-Brautbar et al., 2012; Lu et al., 2016; Sun et al., 2012; Wang et al., 2012). In this manner, TIPE2 acts as a molecular bridge between inflammation and cancer. However, whether TIPE2 is involved in regulating MDSC function is unknown. In this report, we describe an unexpected connection between TIPE2 and MDSC in tumorigenesis.

Results

TIPE2 deletion reduced tumor progression in mice in an MDSC-dependent manner

To explore the potential roles of TIPE2 in tumor growth, we compared tumor growth kinetics and the survival of WT and TIPE2-deficient (*Tipe2*$^{-/-}$) C57BL/6 mice s.c. injected with LLC (Lewis lung carcinoma) and B16F10 melanoma cells. In both tumor models, decreased tumor growth (Fig. 1 A) and extended mouse survival (Fig. 1 B) were noted in *Tipe2*$^{-/-}$ mice, compared with WT controls. In addition, decreased tumor and spleen size and increased tumor cell necrosis were observed in tumors from *Tipe2*$^{-/-}$ mice To test the roles of MDSCs in these mice, we depleted MDSCs using an anti-Gr-1 antibody (Mundy-Bosse et al., 2011). MDSC depletion significantly reduced LLC tumor growth in WT mice but, unexpectedly, enhanced it in *Tipe2*$^{-/-}$ mice (Fig. 1 C). Similar results were observed in B16F10 tumor-bearing mice (Fig. S1 E). In addition, depletion of MDSCs prolonged the survival of LLC-bearing WT mice but shortened the survival of LLC-bearing *Tipe2*$^{-/-}$ mice (Fig. 1 D), suggesting a change in MDSC function from pro-tumoral in WT mice to antitumoral in *Tipe2*$^{-/-}$ mice. Thus, deletion of TIPE2 induced antitumor activity in mice in an MDSC-dependent manner.

TIPE2-deficient MDSCs inhibited tumor growth in mice

We asked if *Tipe2*$^{-/-}$ MDSCs directly mediated antitumor responses. LLC cells were mixed at a 1:1 ratio with MDSCs isolated from WT or *Tipe2*$^{-/-}$ mice bearing LLC tumors and injected s.c. into WT or *Tipe2*$^{-/-}$ mice, with LLC alone as the control (Thevenot et al., 2014). Coinjection of tumor cells with *Tipe2*$^{-/-}$ MDSCs, but not WT MDSCs, into WT mice significantly delayed tumor growth compared with LLC alone, whereas coinjection of tumor cells with WT MDSCs, but not *Tipe2*$^{-/-}$ MDSCs, into *Tipe2*$^{-/-}$ mice partially restored tumor growth compared with LLC alone (Fig. 1 E).

We next evaluated the therapeutic effect of *Tipe2*$^{-/-}$ MDSCs in established tumors. MDSCs isolated from WT or *Tipe2*$^{-/-}$ mice bearing LLC tumors were injected i.v. into WT mice on days 3 and 6 after s.c. LLC injection, with LLC alone as the control. Adoptive transfer of *Tipe2*$^{-/-}$ MDSCs after LLC injection significantly diminished tumor growth compared with LLC alone, whereas adoptive transfer of WT MDSCs had no detectable effect (Fig. 1 F). These results indicate that TIPE2-deficient MDSCs promoted, but did not inhibit, antitumor effects. In both WT and *Tipe2*$^{-/-}$ mice, CD8 but not CD4 T cells played a role in suppressing tumor growth (Fig. 1 G). TIPE2 deficiency reduced not only in situ tumor growth but also tumor metastasis into the lung (Figs. 1 H and S1 F).

TIPE2 deletion increased the accumulation, but blocked the inhibitory function, of MDSCs

We then asked whether TIPE2 affected the distribution and function of MDSCs. By flow cytometry, we found that the percentages of several CD45$^+$ subsets, including G-MDSCs, M-MDSCs, CD4$^+$ T cells, and CD8$^+$ T cells, were increased in tumors of LLC-bearing *Tipe2*$^{-/-}$ mice compared with those of WT controls (Figs. 2 A and S2, A and B). In addition, the percentages of MDSCs were also increased in the spleen, lung, and liver, but not bone marrow (BM), of LLC-bearing *Tipe2*$^{-/-}$ mice compared with those of WT controls (Fig. 2 B). However, the percentages of dendritic cells (DCs), macrophages, B cells, and natural killer (NK) cells in tumors were not different between LLC-bearing WT and *Tipe2*$^{-/-}$ mice (Figs. 2 A and S2, A and B).

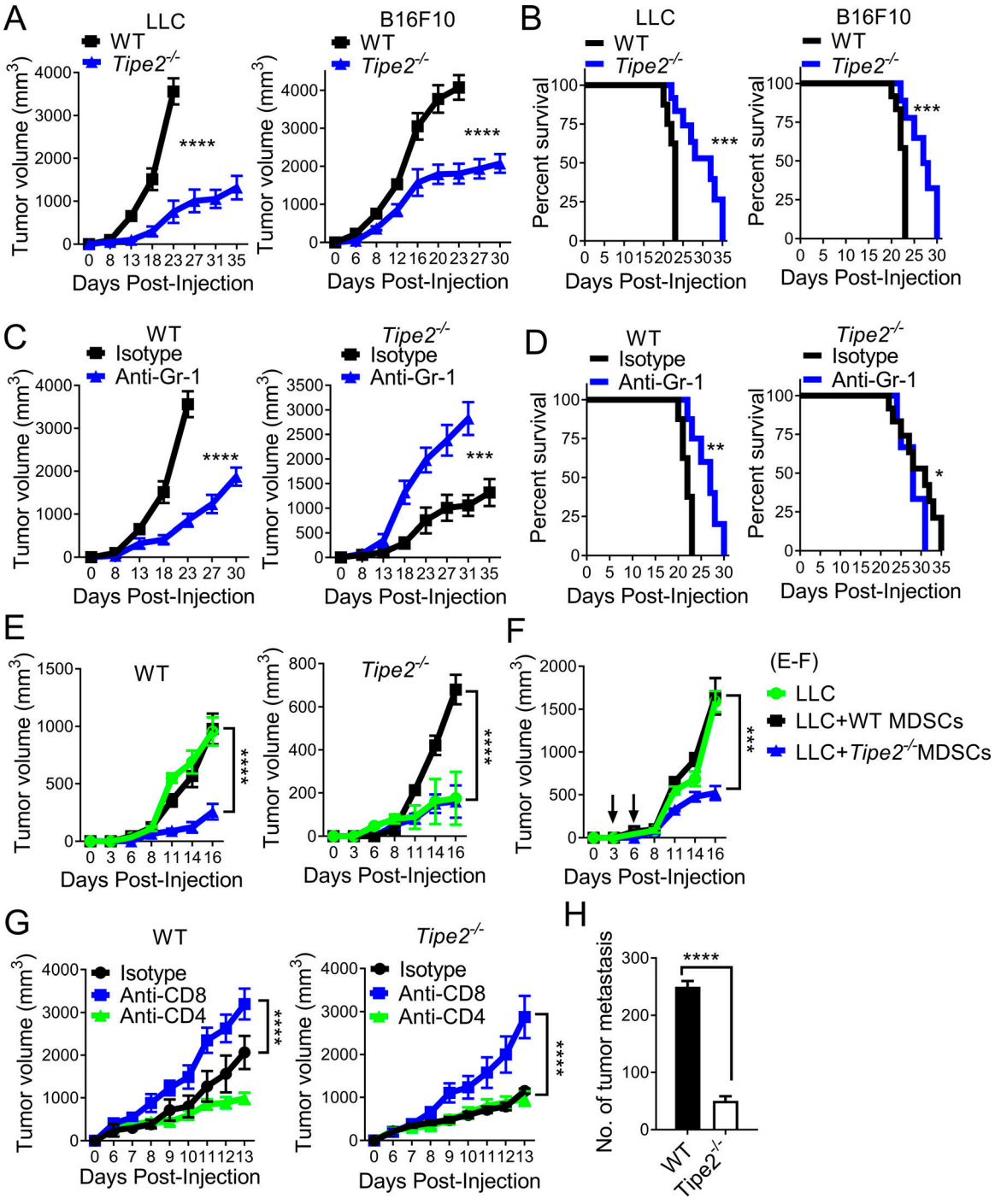

Figure 1. **TIPE2 deficiency significantly reduced tumor growth in mice in an MDSC-dependent manner. (A and B)** Tumor growth curve (A) and mouse survival rate (B) of WT and *Tipe2*$^{-/-}$ C57BL/6 mice (n = 10 mice/group) injected s.c. on day 0 with LLC lung carcinoma or B16F10 melanoma cells as indicated. **(C and D)** Tumor growth curve (C) and mouse survival rate (D) of WT and *Tipe2*$^{-/-}$ C57BL/6 mice (n = 10 mice/group) injected s.c. on day 0 with LLC lung carcinoma cells and that received i.p. injections of either anti-Gr-1 (RB6-8C5) or isotype control antibody once every 3 d. **(E)** Tumor growth in WT (left) and *Tipe2*$^{-/-}$ (middle) mice (n = 6 mice/group) injected s.c. on day 0 with LLC cells alone or coinjected with LLC cells plus purified splenic MDSCs from WT or *Tipe2*$^{-/-}$ mice, mixed at a 1:1 ratio. **(F)** Tumor growth in WT mice (n = 6 mice/group) injected s.c. on day 0 with LLC cells, with or without subsequent i.v. injections, on days 3 and 6, of splenic WT or *Tipe2*$^{-/-}$ MDSCs as indicated. **(G)** Tumor growth in WT and *Tipe2*$^{-/-}$ C57BL/6 mice (n = 10 mice/group) injected s.c. on day 0 with LLC cells and that received i.p. injections of anti-CD4, anti-CD8, or isotype control antibodies twice every week. **(H)** Number of lung tumors assessed 14 d after i.v. injection of B16F10 cells into WT and *Tipe2*$^{-/-}$ C57BL/6 mice (n = 8 mice/group). Results are pooled from three (A–D, G, and H) or two (E and F) independent experiments. Error bars show means ± SEM. Unpaired Student's t test was used for A, C, and E–H. The log-rank test was used for B and D. *, P < 0.05; **, P < 0.01; ***, P < 0.001; ****, P < 0.0001.

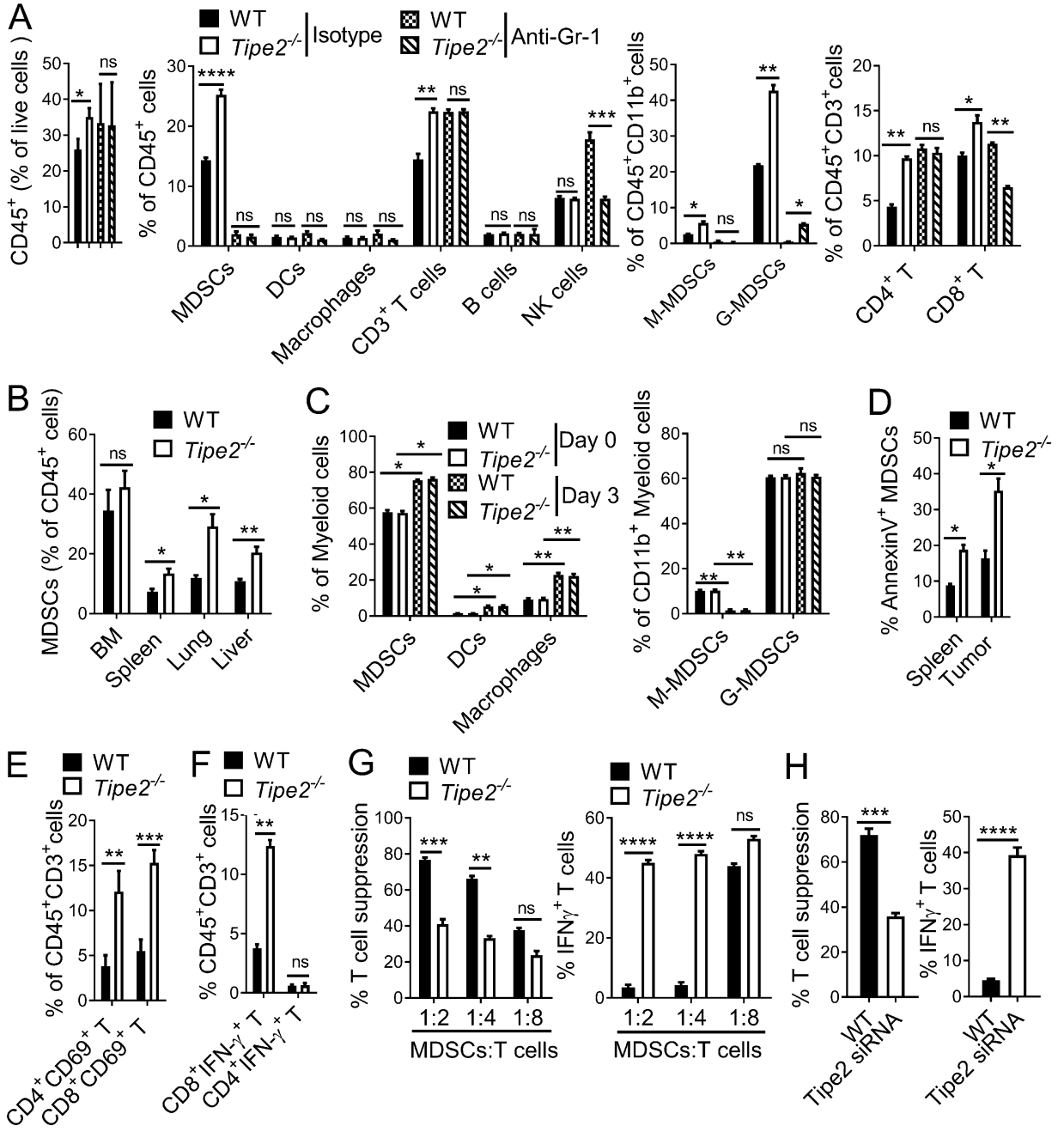

Figure 2. **TIPE2 conferred the immunosuppressive function of MDSCs. (A)** Percentages of indicated leukocyte subsets among live cells isolated from tumors of WT and *Tipe2*$^{-/-}$ mice injected s.c. on day 0 with LLC cells and that received i.p. injections, starting on day 7, of either anti-Gr-1 (RB6-8C5) or isotype control antibody once every 3 d, as determined by flow cytometry 17 d after LLC cell injection. Leukocytes were CD45$^+$; MDSCs were CD45$^+$CD11b$^+$Gr-1$^+$; G-MDSCs were CD45$^+$CD11b$^+$Ly6G$^+$Ly6C^{low}; M-MDSCs were CD45$^+$CD11b$^+$Ly6G$^-$Ly6C^{high}; DCs were CD45$^+$CD11b$^+$CD11c$^+$; macrophages were CD45$^+$CD11b$^+$F4/80$^+$; CD3$^+$ T cells were CD45$^+$CD3$^+$NK1.1$^-$; CD4$^+$ T cells were CD45$^+$CD3$^+$CD4$^+$CD8$^-$; CD8$^+$ T cells were CD45$^+$CD3$^+$CD4$^-$CD8$^+$; B cells were CD45$^+$CD3$^-$CD19$^+$; and NK cells were CD45$^+$CD3$^-$NK1.1$^+$. Gating strategies are shown in Fig. S2, A and B. **(B)** Percentages of MDSCs (CD11b$^+$Gr-1$^+$CD45$^+$) in BM, spleen, lung, and liver of WT and *Tipe2*$^{-/-}$ mice 17 d after LLC cell injection. **(C)** BM cells isolated from WT and *Tipe2*$^{-/-}$ mice were cultured in the presence of GM-CSF for 3 d. The percentages of the indicated myeloid subsets before (day 0) and after the in vitro culture (day 3) were determined by flow cytometry. Gating strategies are shown in Fig. S3 A. **(D)** Percentages of annexin V$^+$ MDSCs in the spleens and tumors of WT and *Tipe2*$^{-/-}$ mice 17 d after LLC cell injection. **(E)** Percentages of CD69$^+$CD4$^+$ T cells and CD69$^+$CD8$^+$ T cells among CD45$^+$CD3$^+$ cells isolated from tumors of WT and *Tipe2*$^{-/-}$ mice injected s.c. with LLC cells 17 d earlier, as determined by flow cytometry. **(F)** Percentages of IFNγ-expressing CD8$^+$ and CD4$^+$ T cells among splenic CD45$^+$CD3$^+$ cells of WT and *Tipe2*$^{-/-}$ mice injected s.c. with B16F10 cells 16 d earlier, as determined by flow cytometry. Cells were activated in vitro with anti-CD3 and anti-CD28 for 48 h before testing. **(G)** Percentage of T cell suppression (left) and IFNγ-expressing T cells (right) in co-cultures of MDSCs and CFSE-labeled CD3$^+$ T cells at the indicated ratios, as determined by flow cytometry. MDSCs were isolated from spleens of WT and *Tipe2*$^{-/-}$ mice injected s.c. with LLC cells 17 d earlier. **(H)** Percentage of T cell suppression (left) and IFNγ-expressing T cells (right) in co-cultures of CFSE-labeled CD3$^+$ T cells and WT or Tipe2 knockdown (*Tipe2* siRNA) MDSCs at an MDSC:T cell ratio of 1:4, as determined by flow cytometry. MDSCs were generated from the BM of C57BL/6 mice and treated with pLKO.1-TRC-Tipe2 siRNA lentivirus (for *Tipe2* siRNA group) or control siRNA lentivirus (for WT group) before testing. Representative results from three independent experiments are shown (n = 6 mice/group; A–H). Results are expressed as mean ± SEM. Unpaired Student's t test for A–H. *, P < 0.05; **, P < 0.01; ***, P < 0.001; ****, P < 0.0001; ns, not significant.

MDSC depletion by anti-Gr-1 treatment almost completely depleted MDSCs in tumors of LLC-bearing WT and *Tipe2*$^{-/-}$ mice, while the percentages of other myeloid cells such as DCs and macrophages of LLC-bearing WT and *Tipe2*$^{-/-}$ mice were not affected (Figs. 2 A and S2, A and B). MDSC depletion increased the percentages of CD45$^+$ leukocyte subsets, including NK cells, CD3$^+$ T cells, CD4$^+$ T cells, and CD8$^+$ T cells in LLC-bearing WT mice but significantly decreased the percentages of CD8$^+$ T cells in LLC-bearing *Tipe2*$^{-/-}$ mice, while the percentages of other CD45$^+$ leukocytes such as CD3$^+$ T cells, CD4$^+$ T cells, B cells, and NK cells in tumors of LLC-bearing *Tipe2*$^{-/-}$ mice were not affected (Figs. 2 A and S2, A and B). Compared with the WT controls, MDSC depletion also decreased the percentages of NK cells and CD8$^+$ T cells of LLC-bearing *Tipe2*$^{-/-}$ mice; however, the percentages of other CD45$^+$ leukocytes such as CD3$^+$ T cells, CD4$^+$ T cells, and B cells in tumors were not different between LLC-bearing WT and *Tipe2*$^{-/-}$ mice (Figs. 2 A and S2, A and B).

To explore the potential mechanism of increased MDSC accumulation in *Tipe2*$^{-/-}$ mice, we investigated the effect of TIPE2 on the differentiation potential of BM precursors to become MDSCs or other myeloid subpopulations with known proliferation capacity and apoptosis of MDSCs. In the in vitro BM cell differentiation assays, *Tipe2*$^{-/-}$ BM precursors showed a similar potential to differentiate into MDSCs or other myeloid subpopulations (DCs and macrophages) with known proliferation capacity compared with WT controls (Figs. 2 C and S3 A). However, increased annexin V and cleaved caspase 3 signals were also detected in tumor MDSCs of *Tipe2*$^{-/-}$ mice, compared with those of WT controls (Figs. 2 D and S3, B and C). These results suggest that TIPE2 deficiency increased the turnover of MDSCs in *Tipe2*$^{-/-}$ mice.

Neither WT nor *Tipe2*$^{-/-}$ MDSCs displayed high levels of cytotoxicity when mixed with tumor cells in vitro (Fig. S3 D). The frequencies of activated CD69$^+$CD4$^+$ and CD69$^+$CD8$^+$ T cells were significantly increased in B16F10-bearing *Tipe2*$^{-/-}$ mice, compared with those in WT controls (Figs. 2 E and S3 E). Furthermore, an elevated number of CD8$^+$ T cells, but not CD4$^+$ T cells, producing IFNγ was observed in tumor-bearing *Tipe2*$^{-/-}$ mice compared with WT controls (Figs. 2 F and S3 F). These results indicated that *Tipe2*$^{-/-}$ MDSCs may regulate antitumor immunity through T cells.

Indeed, when tested in vitro, tumor-derived MDSCs from *Tipe2*$^{-/-}$ mice had a reduced capacity to block T cell proliferation or IFNγ production, compared with those from WT controls (Fig. 2 G). Importantly, siRNA-mediated knockdown of TIPE2 in BM-derived MDSCs also significantly reduced their ability to block T cell proliferation and T cell production of IFNγ, compared with the controls (Fig. 2 H), suggesting that TIPE2 promoted MDSC function in a cell-intrinsic manner.

TIPE2 specified the pro- and antitumoral gene expression in MDSCs

We next determined whether TIPE2 controlled the expression of MDSC signature genes using several methods, including RNA sequencing (RNA-seq), reverse transcription quantitative PCR (RT-qPCR), biochemical assays, ELISA, and flow cytometry. We found that loss of TIPE2 caused a significant change in gene expression profiles important for MDSC function. Interestingly, genes with increased expression in *Tipe2*$^{-/-}$ tumoral MDSCs were enriched for M1 proinflammatory signatures (Pan et al., 2017), compared with those in WT controls (Fig. S4 A). By RT-PCR, we further confirmed the increase of a number of M1 immune stimulatory signature genes (including Il12p35, Il12p40, Tnfα, Inos, Arg2, Nfkb1, Cd80, Irf7, and Ccl5) and the decrease of a number of M2 immunosuppressive signature genes (including Arg1, Il10, Il6, P67^{phox}, and Tgfb1) in Tipe2$^{-/-}$ tumor MDSCs (Fig. 3 A). Specifically, compared with WT MDSCs, *Tipe2*$^{-/-}$ MDSCs exhibited significant defects in the expression of M2 immunosuppressive signature proteins such as arginase 1 (ARG1), ROS, PD-L1, IL-6, IL-10, TGF-β, and IL-4Rα (Fig. 3, B–E; and Fig. S4, B and C). By contrast, the expression of immune stimulatory molecules such as MHC class I and II, costimulatory molecules CD80 and CD86, TNF-α, IL-12, and NF-κB1 was increased in *Tipe2*$^{-/-}$ MDSCs compared with WT MDSCs (Fig. 3, A, D, and E; and Fig. S4 B). The latter molecules are known to be important for T cell activation. These results indicate that lack of TIPE2 converted MDSCs from an immunosuppressive phenotype to a stimulatory one.

TIPE2 regulated MDSC function via C/EBPβ

C/EBPβ plays a crucial role in MDSC development and function (Marigo et al., 2010). Although similar levels of C/EBPβ mRNA were found in tumor-derived WT and *Tipe2*$^{-/-}$ MDSCs (Fig. 4 A), the expression of C/EBPβ-LAP*, C/EBPβ-LAP, and inhibitory C/EBPβ isoform LIP proteins was markedly reduced in *Tipe2*$^{-/-}$ MDSCs compared with WT MDSCs (Fig. 4 B). C/EBPβ transactivation activity is controlled by phosphorylation, which is mediated by the AKT–GSK-3β or ERK signal pathway (Maekawa et al., 2015; Shen et al., 2009). TIPE2 deletion in MDSCs increased the abundance of phospho-AKT (S473) and phospho-GSK-3β (Ser9), but not that of phosphor-ERK (Thr202/Tyr204; Fig. 4 C). The total phosphorylation level of C/EBPβ (as determined by an anti-phosphothreonine antibody), but not the level of phospho-C/EBPβ (Thr188), was significantly increased in *Tipe2*$^{-/-}$ MDSCs compared with WT MDSCs (Fig. 4 D).

Consistent with these findings, C/EBPβ binding to its target genes *Il6* and *Il10*, as measured by chromatin immunoprecipitation (ChIP), was significantly reduced in *Tipe2*$^{-/-}$ MDSCs compared with WT MDSCs (Fig. 4 E). Notably, enforced expression of C/EBPβ-LAP in *Tipe2*$^{-/-}$ MDSCs partially rescued their immunosuppressive function (Fig. 4 F) and *Il6* expression (Fig. 4 G), suggesting that TIPE2 regulated MDSC function via C/EBPβ.

Tipe2$^{-/-}$ MDSCs exhibited not only reduced IL-6 expression but also diminished phospho-STAT3 signals (Fig. 5 A). However, the expression of IL-6 receptors CD126 and CD130 was similar in tumor-derived MDSCs of WT and *Tipe2*$^{-/-}$ mice (Fig. 5 B). To determine the effect of reduced IL-6 expression in *Tipe2*$^{-/-}$ mice, B16F10 cells overexpressing IL-6 (B16F10-*IL-6*) were injected into WT and *Tipe2*$^{-/-}$ mice. Ectopic expression of IL-6 restored tumor growth in *Tipe2*$^{-/-}$ mice (Fig. 5 C), and B16F10-*IL-6* tumor-derived MDSCs from *Tipe2*$^{-/-}$ mice were equally suppressive as WT MDSCs (Fig. 5 D). Furthermore, the decreased levels of phospho-STAT3 in *Tipe2*$^{-/-}$ MDSCs were partially restored after ectopic expression of IL-6 in tumor cells (Fig. 5 E). These results suggest that IL-6, which is controlled by C/EBPβ, plays an important role in TIPE2-mediated pro-tumoral effects.

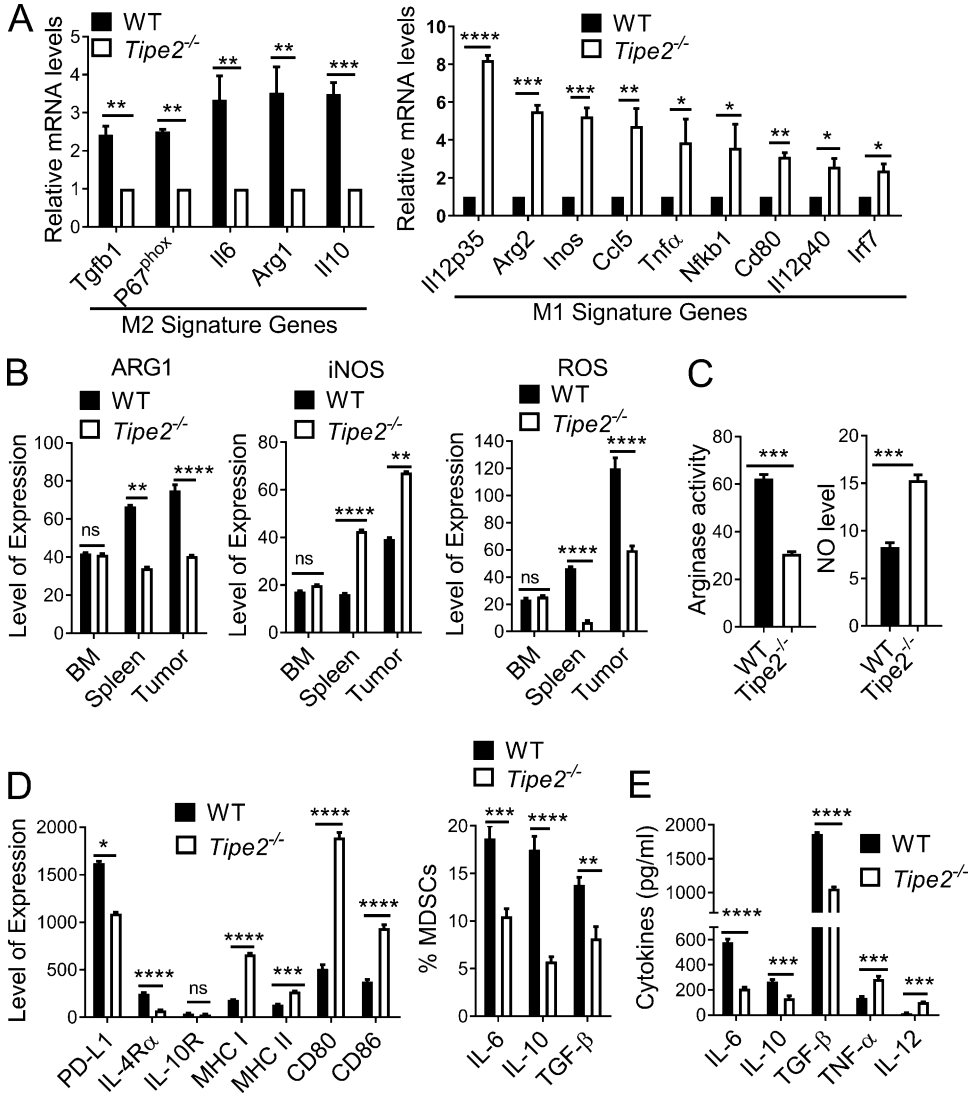

Figure 3. **TIPE2 specified gene expression patterns of MDSCs. (A)** RT-qPCR analyses of mRNA abundance of M1 or M2 signature genes in WT and *Tipe2*$^{-/-}$ MDSCs isolated by FACS from the tumors of C57BL/6 mice that were injected s.c. with B16F10 cells 16 d earlier (n = 3 mice/group). PCR values were normalized to the internal β-actin signal. The values of the *Tipe2*$^{-/-}$ MDSCs were set as 1 (left), and the values of the WT MDSCs were set as 1 (right). **(B)** Flow cytometry analysis of mean fluorescence intensity (× 10^2) of the indicated proteins in WT and *Tipe2*$^{-/-}$ MDSCs isolated by FACS from the tumors, BM, and spleens of C57BL/6 mice that were injected s.c. with LLC cells 17 d earlier (n = 6 samples per group). **(C)** Arginase enzyme activity (U/liter) and NO levels (μmol/liter) of MDSCs isolated by FACS from the tumors of C57BL/6 mice that were injected s.c. with LLC cells 17 d earlier. **(D)** The mean fluorescence intensity and percentages of MDSCs expressing the indicated proteins as determined by flow cytometry. MDSCs were isolated by FACS from the tumors of WT and *Tipe2*$^{-/-}$ C57BL/6 mice that were injected s.c. with B16F10 cells 17 d earlier. They were stimulated with LPS (1 μg/ml) for 6 h before the test. **(E)** Cytokine abundance as determined by ELISA in the whole-cell extracts of MDSCs isolated by FACS from the tumors of WT and *Tipe2*$^{-/-}$ C57BL/6 mice that were injected s.c. with B16F10 cells 16 d earlier. Data are means ± SEM pooled from three independent experiments (A and B) or from one representative of three independent experiments (C–E, n = 6 samples per group). Unpaired student t test for A–E. *, P < 0.05; **, P < 0.01; ***, P < 0.001; ****, P < 0.0001; ns, not significant.

Pharmacological inhibition of ROS decreased TIPE2 expression in MDSCs and reduced tumor growth in mice

To determine whether tumor-derived factors regulated TIPE2 expression in MDSCs, BM-MDSCs were treated with tumor explant supernatant (TES), IL-6, hydrogen peroxide (H_2O_2), and L-arginine, and their TIPE2 levels were measured by immunoblotting. TES, IL-6, and to a lesser degree, H_2O_2 and L-arginine, all markedly induced TIPE2 expression in MDSCs (Fig. 6 A). Interestingly, TES-induced TIPE2 expression was blocked by ROS inhibitor *N*-acetyl cysteine (L-NAC) but not ARG1 inhibitor N^{ω}-hydroxy-nor-arginine (nor-NOHA) or iNOS inhibitor L-N^{G}-monomethyl arginine citrate (L-NMMA; Qin et al., 2013; Yan et al., 2013; Yang et al., 2015; Fig. 6 B). Moreover, treatment of tumor-bearing WT mice, but not *Tipe2*$^{-/-}$ mice, with L-NAC resulted in a significant decrease in tumor growth (Fig. 6 C). The combination of L-NAC with immune checkpoint inhibitor anti-PD-1, however, did not enhance its antitumor effect in WT or *Tipe2*$^{-/-}$ tumor-bearing mice (Fig. 6 D). L-NAC treatment also impaired MDSC function (Fig. 6 E) and reduced the expression of *Tipe2* and *Arg1* (Fig. 6 F); the abundance of ROS in tumor-derived MDSCs (Fig. 6 G). p47^{phox}, a key component of NADPH oxidases (NOXs) that is responsible for ROS

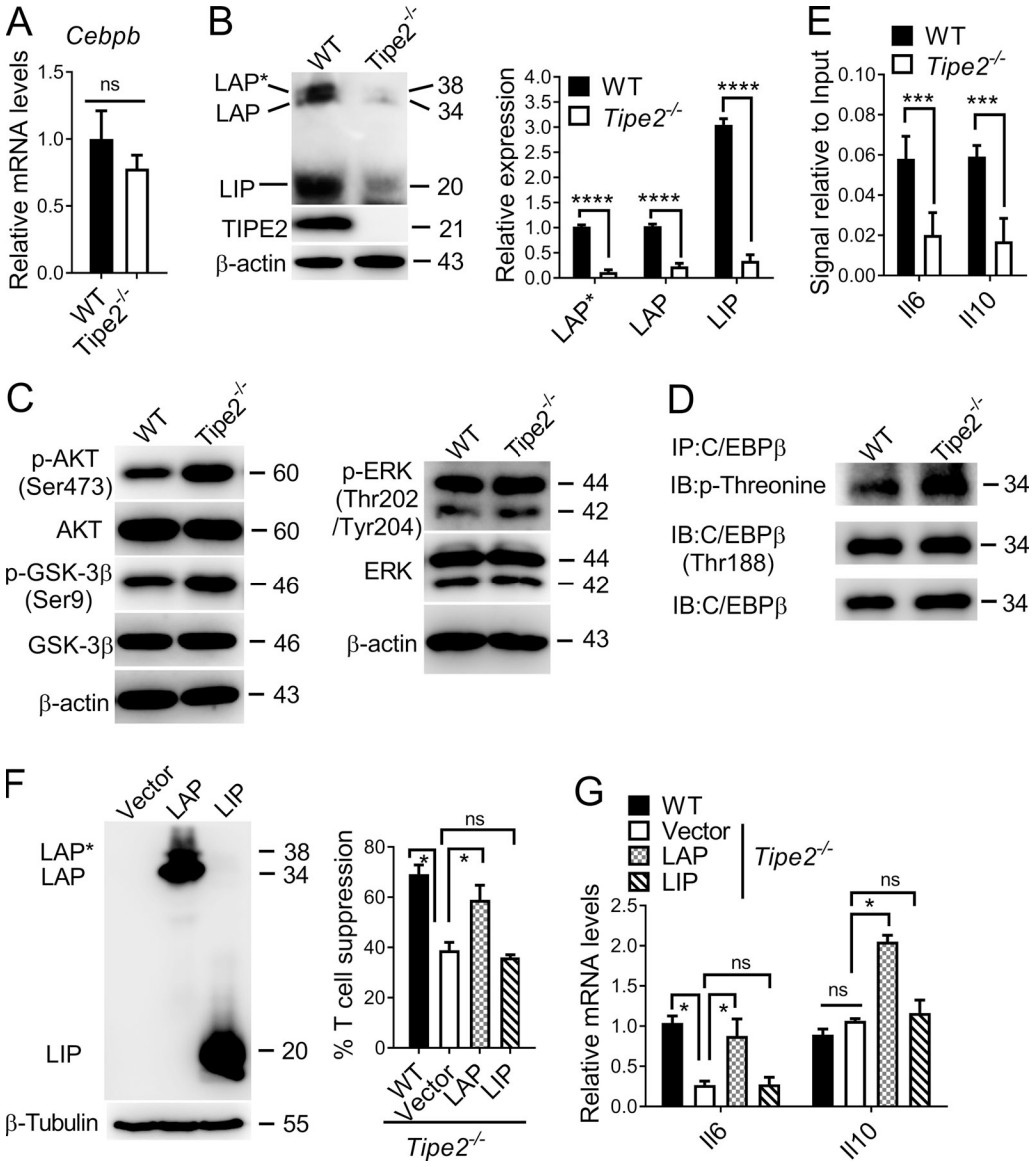

Figure 4. **TIPE2 controlled MDSC function through C/EBPβ. (A and B)** C/EBPβ expression as determined by RT-qPCR (A) and immunoblotting (B) in MDSCs isolated from tumors of WT and *Tipe2*$^{-/-}$ C57BL/6 mice that were injected s.c. with B16F10 cells 16 d earlier. Right graph of B shows levels of C/EBPβ LAP, LAP*, and LIP proteins as determined by densitometry. Data are means ± SEM pooled from three independent experiments (n = 6 mice per group per experiment). Molecular weights: LAP* = 38 kD; LAP = 34 kD; LIP = 20 kD. **(C)** Expression levels of the indicated proteins as determined by immunoblotting in MDSCs isolated from tumors of WT and *Tipe2*$^{-/-}$ C57BL/6 mice that were injected s.c. with B16F10 cells 16 d earlier. **(D)** Abundance of the indicated molecules as determined by immunoblotting (IB) in the immunoprecipitates (IP) of WT and *Tipe2*$^{-/-}$ MDSCs isolated from the spleens of B16F10 tumor-bearing mice; the immunoprecipitates were collected with protein G agarose beads after incubating the MDSC lysates with anti-C/EBPβ. **(E)** ChIP PCR analyses of the *Il6* and *Il10* promoter regions with anti-C/EBPβ for tumor-derived WT and *Tipe2*$^{-/-}$ MDSCs isolated from B16F10 tumor-bearing mice. **(F and G)** C/EBPβ–LAP rescue of the functional deficiency of *Tipe2*$^{-/-}$ MDSCs. **(F)** Left: Immunoblot analysis of HEK293T cells treated with or without pLVX-IRES-ZsGreen1/LAP (pLVX-LAP), pLVX-IRES-ZsGreen1/ LIP (pLVX-LIP), or pLVX-IRES-ZsGreen1 (pLVX- Vector) viruses. Right: Percentage of T cell suppression mediated by WT MDSCs and *Tipe2*$^{-/-}$ MDSCs infected with pLVX-Vector control, pLVX-LAP, or pLVX-LIP lentiviruses at an MDSC:T cell ratio of 1:4. **(G)** RT-qPCR results of *Il6* and *Il10* gene expression levels in WT MDSCs and *Tipe2*$^{-/-}$ MDSCs infected with pLVX-Vector control, pLVX-LAP, or pLVX-LIP lentiviruses. All MDSCs were isolated from the spleens of B16F10 tumor-bearing mice 16 d after tumor cell injection. For C–G, data are means ± SEM and are from a representative experiment of three; n = 6 mice per group. Unpaired Student's t test for A, B, and E–G. *, P < 0.05; ***, P < 0.001; ****, P < 0.0001; ns, not significant.

production in MDSCs (Corzo et al., 2009), was down-regulated by L-NAC (Fig. 6 H); and its knockdown by shRNA blocked TIPE2 expression in MDSCs (Fig. 6 I). In addition, blocking ROS by L-NAC also inhibited C/EBPβ LAP* and LAP expression (Fig. 6 J). These results indicate that TIPE2 may be manipulated pharmacologically to treat cancer.

TIPE2 conferred immunosuppressive function of human MDSCs, and its high-level expression in MDSCs of lung cancer patients correlated with poor long-term survival

Although M-MDSCs (HLA-DR$^{-/low}$CD33^{+}CD14^{+}CD66b^{-}) and G-MDSCs (HLA-DR$^{-/low}$ CD33^{+}CD14$^{-/low}$CD66b^{+}) have been described in humans, it has been suggested that both subsets

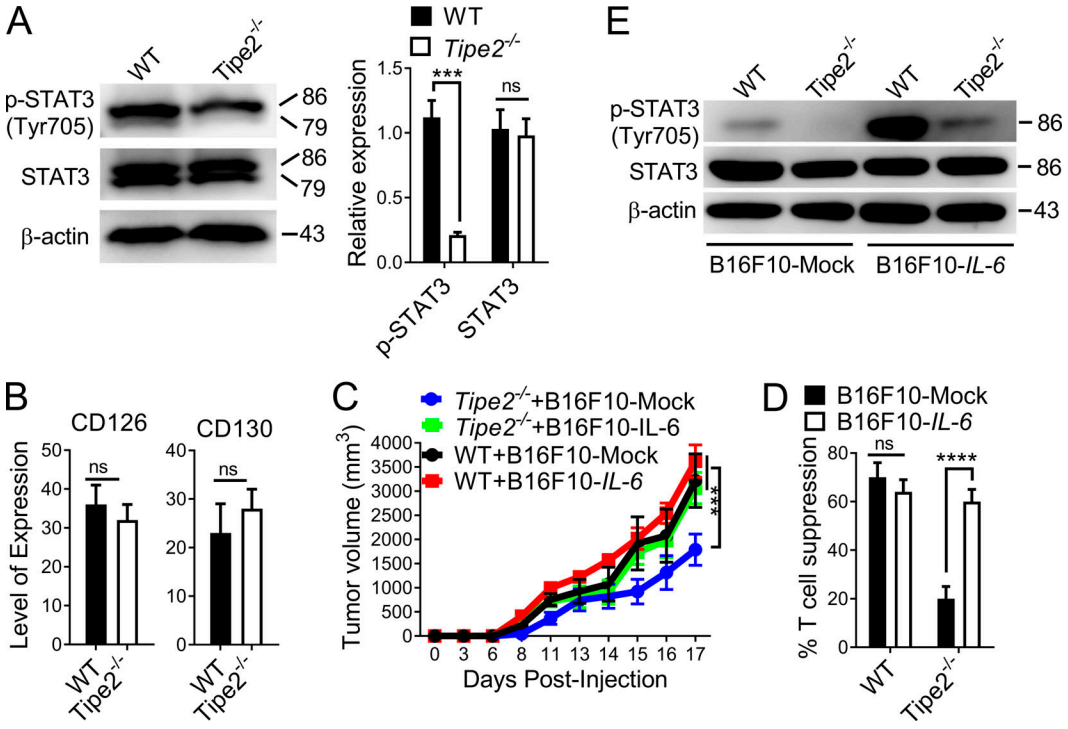

Figure 5. **IL-6–mediated rescue of the functional deficiency of *Tipe2*$^{-/-}$ MDSCs. (A)** Expression levels of the indicated proteins in WT and *Tipe2*$^{-/-}$ tumor-derived MDSCs as determined by immunoblotting (left) and densitometric analysis of the immunoblots (right). **(B)** Histograms of CD126 and CD130 expression by CD45^{+}CD11b^{+}Gr-1^{+} tumor-derived MDSCs from WT and *Tipe2*$^{-/-}$ B16F10 tumor-bearing mice. **(C)** Tumor growth in WT and *Tipe2*$^{-/-}$ mice injected with mock or IL-6–expressing B16F10 cells. **(D)** T cell suppression by tumor-derived MDSCs from WT and *Tipe2*$^{-/-}$ mice injected s.c. with mock or IL-6–expressing B16F10 cells, at an MDSC:T cell ratio of 1:4. **(E)** Expression levels of the indicated proteins as determined by immunoblotting in tumor-derived MDSCs from WT and *Tipe2*$^{-/-}$ mice injected s.c. with mock or IL-6–expressing B16F10 cells. Data are means ± SEM and are from a representative experiment of three; *n* = 6 mice per group (A, B, D, and E) or *n* = 10 mice per group (C). Unpaired Student's *t* test for A–D. ***, P < 0.001; ****, P < 0.0001; ns, not significant.

originate from HLA-DR^{-}CD33^{+} cells containing mixed groups of MDSCs defined as "early-stage" MDSCs (eMDSCs) comprising more immature progenitors (Bronte et al., 2016). To assess whether TIPE2 affected the phenotype and function of human MDSCs in lung cancer patients, we first analyzed the phenotype and percentages of both subsets in peripheral blood mononuclear cells (PBMCs) by flow cytometry. The percentages of MDSC subsets, including M-MDSCs and G-MDSCs, among HLA-DR^{-}CD33^{+} cells of lung cancer patients were significantly higher than those of healthy donors (HDs; Fig. 7, A and B). TIPE2 expression by M-MDSCs and G-MDSCs of lung cancer patients was significantly higher than that of monocytes and neutrophils, respectively, of HDs (Fig. 7 C), indicating that MDSCs of lung cancer patients overexpressed TIPE2. To establish the roles of human TIPE2 in MDSCs, PBMCs from lung cancer patients were cultured in the presence of human GM-CSF and IL-6 for 2 d, and HLA-DR^{-}CD33^{+} eMDSCs isolated by FACS were infected with control or human TIPE2 (*hTIPE2*) shRNA-encoding lentiviruses. The percentages of G-MDSCs and M-MDSCs among HLA-DR^{-}CD33^{+} cells increased significantly in *hTIPE2* shRNA-treated PBMCs compared with control shRNA-treated PBMCs (Fig. 7 D). Importantly, shRNA-mediated knockdown of TIPE2 in G-MDSCs also significantly reduced their ability to suppress T cell proliferation and T cell production of IFNγ, compared with the controls (Fig. 7 E). In addition, compared with control shRNA-treated G-MDSCs, *hTIPE2* shRNA-treated G-MDSCs exhibited significant defects in the expression of immunosuppressive proteins such as ARG1 and ROS-related p47phox, but more iNOS (Fig. 7 F). *hTIPE2* shRNA-treated G-MDSCs expressed markedly less C/EBPβ-LAP* and C/EBPβ-LAP proteins (Fig. 7 F) and C/EBPβ downstream target molecules IL-6 and IL-10, but more TNF-α (Fig. 7 G), compared with control shRNA-treated G-MDSCs. These results indicate that knockdown of TIPE2 converted human MDSCs from an immunosuppressive phenotype to a stimulatory one.

We next evaluated the relationship between TIPE2 mRNA levels and the presence of MDSCs in human lung cancers using The Cancer Genome Atlas dataset (Cancer Genome Atlas Research Network, 2014). Interestingly, TIPE2 levels significantly correlated with the expression of MDSC-associated surface markers (CD33, CD14) or MDSC-associated genes (IL-10, NOX2) and weakly associated with the expression of C/EBPβ and ARG1 (Spearmanp value: 0.115 and 0.0489, respectively), but only inversely correlated with the expression of iNOS (Spearman p value: −0.0139; Fig. S5 A). To determine the relationship between TIPE2 expression in MDSCs and long-term lung cancer patient survival, we examined TIPE2 expression levels in HLA-DR$^{-/low}$CD33^{+}CD11b^{+}CD14$^{-/low}$CD66b^{+} G-MDSCs of 92 lung cancer patients using multiplexed fluorescence immunohistochemistry (mIHC), which allows analyses of seven-parameter immunofluorescence signals on each sample (Figs. 8 A and S5 B). Patient characteristics are shown

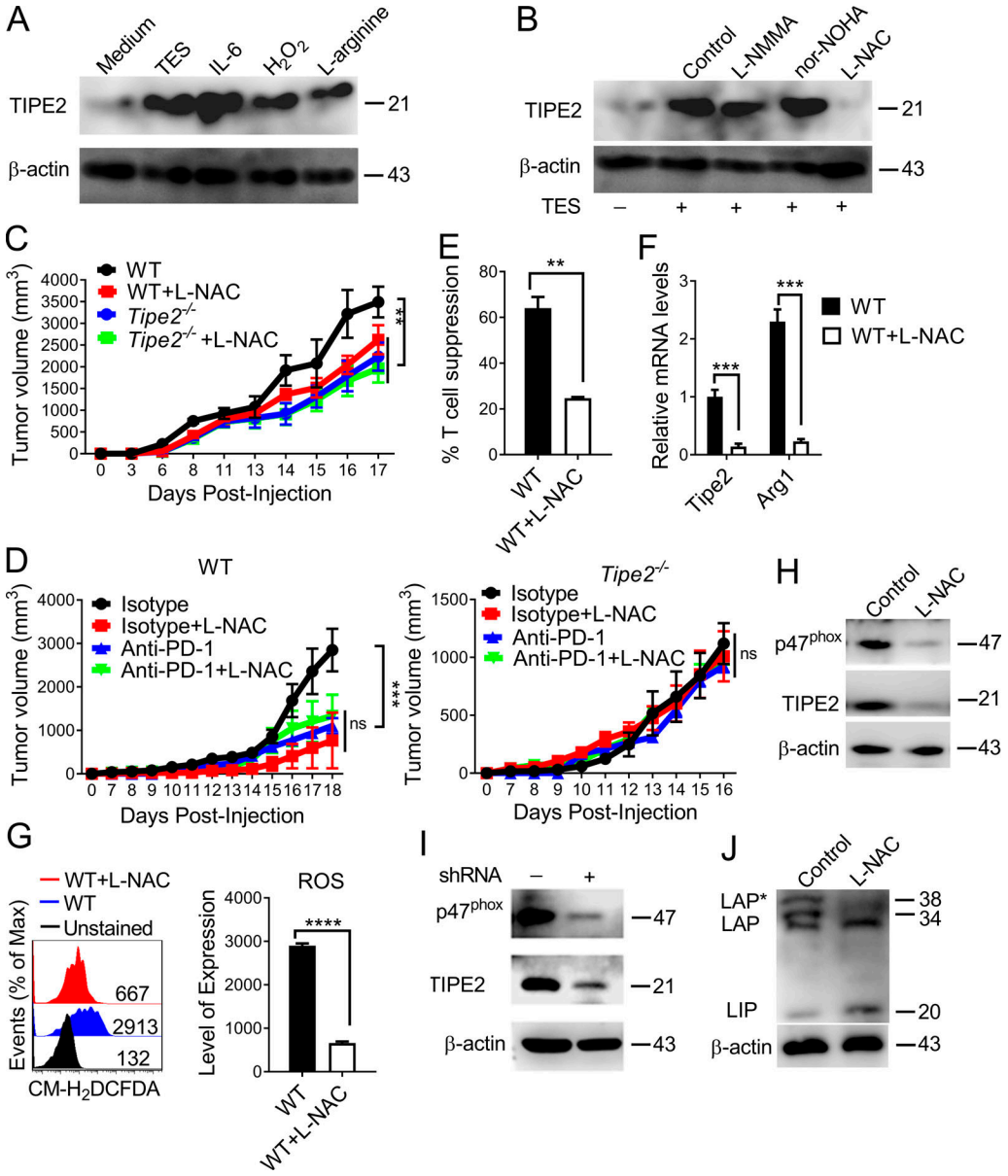

Figure 6. **Tumor-derived ROS-induced TIPE2 expression in MDSCs. (A)** TIPE2 expression in BM-derived MDSCs cultured for 24 h in medium alone or medium containing 40% TES, IL-6 (40 ng/ml), hydrogen peroxide (H_2O_2; 250 mM), and L-arginine (1 mM). TES was collected after culturing B16F10 tumor cells overnight at 1×10^7 cells/ml. **(B)** TIPE2 expression in BM-derived MDSCs cultured with or without 40% TES, 1 mM L-NAC (ROS inhibitor), 100 µM L-NMMA (arginase I inhibitor), or 100 µM nor-NOHA (iNOS inhibitor). **(C)** B16F10 tumor growth in WT and *Tipe2*$^{-/-}$ mice treated i.p. once a day with PBS or 1.5 mg/mouse L-NAC (n = 10 mice per group). **(D)** Tumor growth in WT and *Tipe2*$^{-/-}$ mice injected s.c. on day 0 with B16F10 cells and treated i.p. once a day with PBS or 1.5 mg/mouse L-NAC and that received, starting on day 7, i.p. injections of anti-PD-1 antibodies or isotype control antibodies twice a week for 2 wk (n = 10 mice per group). **(E)** T cell suppression by tumor-derived MDSCs from PBS- or L-NAC–treated B16F10 tumor-bearing mice, at an MDSC:T cell ratio of 1:4 (n = 6 mice per group). **(F)** *Tipe2* and *Arg1* expression in tumor-derived MDSCs from B16F10 mice treated with PBS or L-NAC for 16 d (n = 6 mice per group). **(G)** Flow cytometry analysis of ROS in tumor-derived MDSCs from B16F10 mice treated with PBS or L-NAC for 16 d. Right graph shows means ± SEM, n = 6 mice per group. **(H)** Immunoblot for p47^{phox} and TIPE2 in tumor-derived MDSCs from B16F10 mice treated with PBS or L-NAC for 16 d. **(I)** Immunoblot for p47^{phox} and TIPE2 in B16F10 tumor-derived MDSCs treated with or without pLKO.1-TRC-p47^{phox} shRNA lentiviruses (p47^{phox} shRNA). **(J)** Expression of LAP, LAP*, and LIP in tumor-derived MDSCs from B16F10 mice treated with PBS or L-NAC for 16 d. Molecular weight: LAP* = 38 kD; LAP = 34 kD; LAP = 20 kD. Data are means ± SEM and are from a representative experiment of three (A–D and H–J) or from two independent experiments (E and F). Unpaired Student's t test for C–G. **, P < 0.01; ***, P < 0.001; ****, P < 0.0001; ns, not significant.

in Fig. S5 B. Interestingly, we observed statistically significant inverse correlations between MDSC TIPE2 levels and long-term survival, reinforcing the notion that lung cancer patients with high-TIPE2 MDSCs have poor long-term survival (Fig. 8 B). Taken together, these results support the model wherein ROS-induced TIPE2 controls MDSC immunosuppressive function by releasing IL-6 via C/EBPβ, thereby limiting T cell responses in carcinomas (Fig. S5 C). Thus, targeting TIPE2 represents a new strategy for cancer immunotherapy.

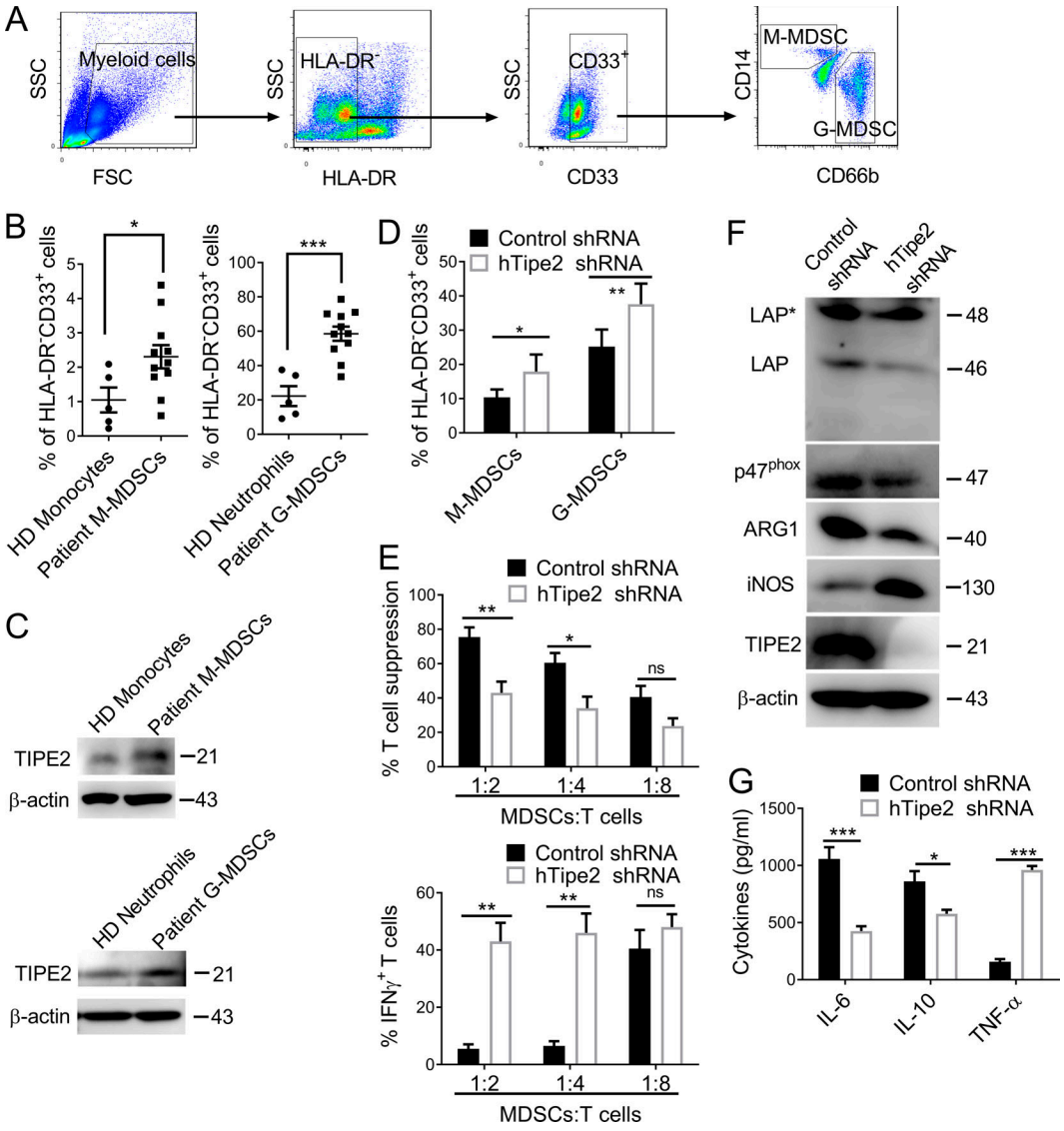

Figure 7. **TIPE2 conferred immunosuppressive function of human MDSCs. (A)** Representative flow cytometry plots illustrating the gating strategy to show human MDSCs, monocytes, and neutrophils from PBMCs of lung cancer patients and HDs. Human neutrophils and G-MDSCs were HLA-DR$^{-/low}$CD33^{+}CD14$^{-/low}$CD66b^{+}; human monocytes and M-MDSCs were HLA-DR$^{-/low}$CD33^{+}CD14^{+}CD66b^{-}. FSC, forward scatter; SSC, side scatter. **(B)** Percentages of indicated patient MDSC subsets and HD monocytes or neutrophils among HLA-DR^{-}CD33^{+} cells of lung cancer patients and HDs, as determined by flow cytometry. **(C)** TIPE2 expression in indicated patient MDSC subsets and HD monocytes or neutrophils from PBMCs of lung cancer patients and HDs. Results are from a representative experiment of three (A–C). HD, n = 5; patients, n = 11 (A–C). **(D–G)** PBMCs from lung cancer patients were cultured in the presence of human GM-CSF and IL-6 for 2 d. HLA-DR^{-}CD33^{+} eMDSCs were infected with control or human TIPE2 (*hTIPE2*) shRNA-encoding lentiviruses and cultured for 2 additional days with GM-CSF and IL-6. **(D)** Percentages of indicated human MDSC subsets among cultured PBMC-derived HLA-DR^{-}CD33^{+} cells, as determined by flow cytometry. **(E)** Percentage of T cell suppression (upper panel) and IFNγ-expressing T cells (lower panel) in co-cultures of HLA-DR$^{-/low}$CD33^{+}CD14$^{-/low}$CD66b^{+} G-MDSCs and CFSE-labeled human CD3^{+} T cells at the indicated ratios, as determined by flow cytometry. G-MDSCs were isolated from PBMC cultures. **(F)** Expression levels of the indicated proteins as determined by immunoblotting in G-MDSCs isolated from PBMC cultures. **(G)** Cytokine abundance as determined by ELISA in the human G-MDSC culture supernatant among PBMC cultures. Data are means ± SEM from one representative of three independent experiments (D–G; n = 6 samples per group). Multiple unpaired Student's t test for B; unpaired Student's t test for D, E, and G. *, P < 0.05; **, P < 0.01; ***, P < 0.001; ns, not significant.

Discussion

Here, we report that TIPE2 is a molecular switch between pro-tumoral MDSCs and antitumoral MDSCs. Tumor-induced inflammation up-regulates TIPE2 expression, which in turn drives MDSC polarization. As a consequence, TIPE2-deficient MDSCs lose their immune-inhibitory functions, and TIPE2-deficient mice have reduced tumor progression and metastasis.

TIPE2 may regulate tumorigenesis directly inside tumor cells or indirectly through immune cells. TIPE2 expression in tumor cells induces cell death (Gus-Brautbar et al., 2012; Lu et al., 2016) and therefore inhibits tumorigenesis (Gus-Brautbar et al., 2012; Sun et al., 2008; Wang et al., 2017; Wu et al., 2016). However, as reported here, by acting on immune cells such as MDSCs, TIPE2 promotes tumorigenesis (Yan et al., 2017). TIPE2 plays

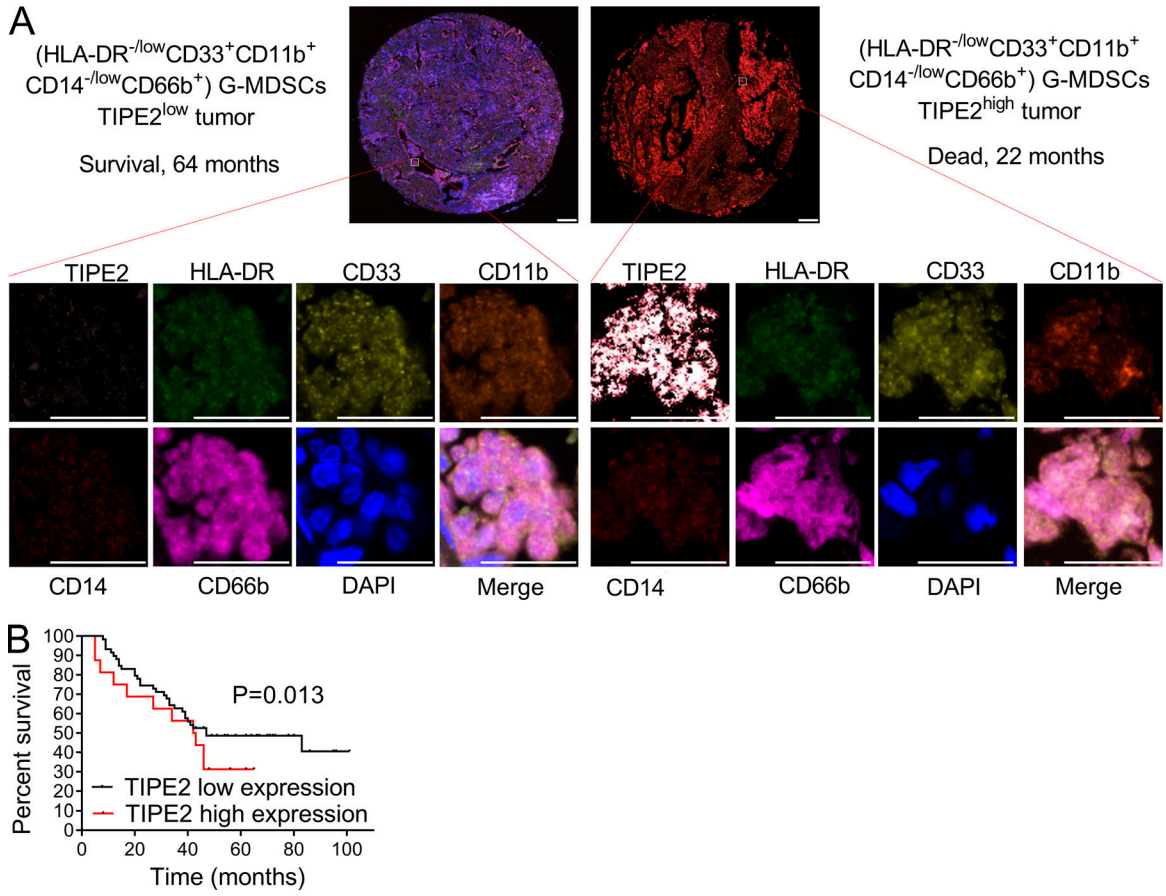

Figure 8. **Lung cancer patients with high-TIPE2 MDSCs have poor long-term survival. (A)** Left: Representative mIHC images of a lung cancer patient with low TIPE2 expression in HLA-DR$^{-/low}$CD33^{+}CD11b^{+}CD14$^{-/low}$CD66b^{+} G-MDSCs (with 1–15% cells positive for TIPE2) who was still alive 64 mo after surgery. Right: Representative mIHC images of a lung cancer patient with high TIPE2 expression in HLA-DR$^{-/low}$CD33^{+}CD11b^{+}CD14$^{-/low}$CD66b^{+} G-MDSCs (with >15% cells positive for TIPE2) who died 22 mo after surgery. TIPE2 high-expressing G-MDSCs are marked by arrows. Nuclei were stained with DAPI. Scale bars, 100 µm. **(B)** Kaplan–Meier analysis of cumulative survival rates of lung cancer patients subdivided by TIPE2 expression in HLA-DR$^{-/low}$CD33^{+}CD11b^{+}CD14$^{-/low}$CD66b^{+} G-MDSCs. Statistical significance was assessed using log-rank test (P = 0.013). TIPE2 low expression, *n* = 58; TIPE2 high expression, *n* = 17; no TIPE2 expression, *n* = 17. The percentages of TIPE2 expression in HLA-DR$^{-/low}$CD33^{+}CD11b^{+}CD14$^{-/low}$CD66b^{+} G-MDSCs of all patients (*n* = 92) are listed in Fig. S5 B.

anti-inflammatory roles by negatively regulating TCR and TLR signaling (Sun et al., 2008). In humans, the down-regulated expression of TIPE2 is inversely associated with systemic autoimmunity, diabetic nephropathy, and hepatitis B infection (Fan et al., 2015; Li et al., 2016; Zhang et al., 2010b). TIPE2 is also implicated in the development of inflammatory diseases such as atherosclerosis, experimental stroke, and acute colitis (Lou et al., 2013, 2014; Zhang et al., 2012).

The induction of TIPE2 expression in MDSCs is mediated by tumor-derived ROS. Tumor cells generate ROS from catabolites of amino acids (arginine, tryptophan, and cysteine), by lipid peroxidation, or by activating endogenous NOXs (Leavy, 2014; Nathan and Cunningham-Bussel, 2013). The latter enzyme has seven isoforms that are differentially expressed in diverse tissues (Tsukagoshi et al., 2010). Among them, NOX1/2 play important roles in immune cells (Tschopp and Schroder, 2010). The subunit p47^{phox} recruits p40^{phox}, p67^{phox}, and small GTPases Rac1/2 to plasma membrane-bound subunit gp91 or NOX1 to form the NOX1 or NOX2 complex (Agudo and Brown, 2016). TIPE2 may also regulate ROS production in neutrophils (Wang et al., 2012) and MDSCs as reported here, but its effect is likely cell specific. Notably, L-NAC treatment decreased the levels of ROS, NOX subunit p47^{phox}, and TIPE2 and blocked the immune-inhibitory function of MDSCs. In addition, shRNA silencing of p47^{phox} in MDSCs led to reduced TIPE2 protein expression, suggesting that once MDSCs are generated, they can use endogenous p47^{phox} to regulate TIPE2 expression. However, the mechanisms of this regulation remain to be established.

Our results indicate that TIPE2 is a critical regulator of C/EBPβ function in MDSCs. TIPE2 increased C/EBPβ abundance and blocked the phosphorylation of C/EBPβ through an AKT- and GSK-3β–dependent, but ERK-independent, mechanism. This finding is consistent with earlier reports that TIPE2 deficiency in T cells and macrophages leads to heightened activation of AKT(Ser473) but not ERK (Fayngerts et al., 2017; Gus-Brautbar et al., 2012; Sun et al., 2008). TIPE2-deficient MDSCs had decreased C/EBPβ binding to the IL-6 promoter but increased C/EBPβ phosphorylation. This finding is consistent with earlier reports that phosphorylation of C/EBPβ by GSK-3β inhibits its DNA-binding and transcriptional activation of target genes

(Maekawa et al., 2015; Shen et al., 2009; Wu et al., 2016). Additionally, the levels of C/EBPβ-LAP and C/EBPβ-LAP* were reduced in *Tipe2*$^{-/-}$ MDSCs, likely further reducing C/EBPβ target gene expression.

In summary, we have discovered that TIPE2 controls MDSC polarization at least in part through C/EBPβ. This regulation is crucial for tumorigenesis because its loss leads to substantially delayed tumor progression. Thus, targeting TIPE2 represents a new strategy for cancer immunotherapy.

Materials and methods

Mice and treatment procedures

All experiments with mice were preapproved by the Animal Care and Use Committee of Shenzhen Institutes of Advanced Technology, Chinese Academy of Sciences. The mice were maintained in the Animal Facilities of Shenzhen Institutes of Advanced Technology, Chinese Academy of Sciences, under pathogen-free conditions. C57BL/6 mice (6–8-wk-old females) were obtained from Guangdong Province Animal Care Facilities. The female TIPE2-deficient (*Tipe2*$^{-/-}$) mice (C57BL/6J background, 6–8 wk old) were described previously (Sun et al., 2008).

LLC and B16F10 cells were obtained from Cell bank, Chinese Academy of Sciences, and were routinely cultured in DMEM supplemented with 10% FBS (Hyclone), 2 mM L-glutamine, 100 U/ml penicillin, and 10 mg/ml streptomycin. All cultures were maintained in a humidified 5% CO_2 incubator at 37°C and routinely passaged when 80–90% confluent. To establish s.c. tumors in *Tipe2*$^{-/-}$ mice, 8 × 10^6 LLC or 4 × 10^6 B16F10 cells were injected s.c. into the mice, and tumor volume was measured and calculated using the formula [(small diameter)^2 × (large diameter) × 0.5] (Corzo et al., 2010). For lung metastasis assays, 1 × 10^6 B16F10 cells were injected i.v., and the number of lung tumors was assessed 14 d later. *IL-6*–expressing B16F10 cells (B16F10-*IL-6*) were generated by transfection using Lipofectamine 3000 (Life Technologies) with vectors coding for IL-6 and GFP (Manderson et al., 2007). GFP-positive B16F10 cells were sorted by FACS (FACSAria III; BD). For MDSC depletion, 200 µg anti-Gr-1 antibody (clone RB6-8C5; BioXcell) was administered i.p. on day 0 and every 3 d for 2 wk. For CD4$^+$ or CD8$^+$ T cell depletion studies, on day 0 after tumor injection, mice were administered i.p. with 400 µg anti-CD4 (clone GK1.5; BioXcell) or anti-CD8 (clone 53.6.72; BioXcell) for 2 wk. Maintenance doses of the depleting antibodies were given twice a week. L-NAC (Sigma-Aldrich) was injected i.p. once a day at a dose of 1.5 mg/mouse.

Patients

Lung cancer patient blood samples were obtained from Shenzhen Second People's Hospital, The First Affiliated Hospital of Shenzhen University. Clinical stages were classified according to the guidelines of the International Union Against Cancer. We purchased the lung cancer tissue array (HLugA180Su03) from Shanghai Outdo Biotech (http://www.superchip.com.cn/). Details on lung cancer patient tissue are provided in Fig. S5 B. All human studies were performed with approval from the ethics committee and Institutional Review Board of Shenzhen Institutes of Advanced Technology.

Cell isolation and purification

Single-cell suspensions were prepared from BM and spleen, followed by red cell removal using ammonium chloride lysis buffer. CD45$^+$ splenic leukocytes were subdivided into the following subsets: CD11b$^+$Gr1$^+$, CD11b$^+$Gr1$^-$, CD11b$^+$CD11c$^+$, CD11b$^+$F4/80$^+$, NK1.1$^+$, CD19$^+$, and CD3$^+$. To obtain single-cell suspensions from tumors, tumors were digested with enzymatic mix containing 0.1 mg/ml hyaluronidase, 2 mg/ml collagenase I, 1 mg/ml DNase I, and 2 mg/ml collagenase IV (Sigma-Aldrich) in RPMI 1640 (Quatromoni et al., 2015). The digested tissue was passed through a 70-µm mesh and washed thoroughly to remove debris. Tumor CD11b$^+$ cells were isolated using magnetic microbeads conjugated with monoclonal rat anti-CD11b antibody. MDSCs were purified on a BD FACSAria III flow cytometer after staining with anti-Gr-1 mAbs, as previously reported (Marigo et al., 2010). The purity of cell populations, which exceeded 90%, was evaluated by flow cytometry.

Flow cytometry

Antibodies specific for the mouse cell surface markers CD19, CD3, CD11b, CD11c, F4/80, Gr-1, Ly6C, Ly6G, MHCI, MHCII, CD80, CD86, PD-L1, IL-4Ra, IL-10R, CD45, CD4, CD8, CD69, CD126, CD130, HLA-DR, CD33, CD14, and CD66b were purchased from BioLegend (all antibodies shown in Table S2). For intracellular staining of IL-6, IL-10 and TGF-β, tumor MDSCs were isolated and stimulated with LPS (1 µg/ml; Sigma-Aldrich) for 6 h, and then stained with the cell surface marker antibodies, followed by fixation, permeabilization with Intracellular Fixation & Permeabilization Buffer Set (eBioscience), and intracellular staining with IL-6, IL-10, and TGF-β antibodies (BioLegend). Flow cytometry data were acquired using Beckman Coulter CytoFLEX or BD FACSCanto II flow cytometer and analyzed with FlowJo software (TreeStar).

MDSC functional assays in vitro and in vivo

For in vitro mouse MDSC function assays, CFSE-labeled CD3$^+$ T cells activated with anti-mouse CD3/CD28 were co-cultured at different ratios with tumor MDSCs isolated from WT and *Tipe2*$^{-/-}$ mice bearing s.c. LLC tumors. For in vitro human MDSC function assays, human CD3$^+$ T cells were sorted from HDs. CFSE-labeled CD3$^+$ T cells activated with anti-human CD3/CD28 were co-cultured at different ratios with HLA-DR$^{-/low}$CD33$^+$CD14$^{-/low}$CD66b$^+$ G-MDSCs isolated from PBMCs of lung cancer patients, which were cultured in the presence of human GM-CSF and IL-6 for 2 d, then infected with control or human *Tipe2* shRNA-encoding lentiviruses and kept for an additional 2 d in culture with the cytokines. T cell proliferation was measured by the dilution of CFSE fluorescence compared with nonactivated T cells. Percentage of T cell suppression was calculated as follows: [(% T cell proliferation of cultures with anti-CD3 and anti-CD28 – % T cell proliferation of cultures with anti-CD3, anti-CD28, and MDSCs)/% T cell proliferation of cultures with anti-CD3 and anti-CD28] × 100. IFNγ expression in T cells was monitored 72 h later by flow cytometry. For in vivo MDSC coinjection experiments, 1 × 10^6 tumor-derived MDSCs were injected with 1 × 10^6 LLC cells s.c. For in vivo MDSC adoptive transfer

experiments, LLC tumor-bearing mice were injected i.v. with control or *Tipe2*$^{-/-}$ tumor MDSCs (3 × 10^6) on days 3 and 6 after tumor injection.

Cytotoxic effects of tumor MDSCs on LLC cells were determined in vitro by lactate dehydrogenase release (Beyotime). Flow cytometry was used to determine the levels of arginase I (with anti-arginase I mAb; Cell Signaling Technology), iNOS (with anti-iNOS mAb; Cell Signaling Technology), and ROS (with CM-H_2DCFDA; Invitrogen) in MDSCs.

BM-derived MDSCs

BM-MDSCs were generated by culturing BM cells for 4 d in the presence of GM-CSF (40 ng/ml; Peprotech). BM-MDSCs were exposed to tumor-derived factors by the addition of 40% B16F10 TES, IL-6 (40 ng/ml; Peprotech), hydrogen peroxide (H_2O_2; 250 mM; Sigma-Aldrich), and L-arginine (1 mM; Sigma-Aldrich) during the last 24 h of culture. In another assay, BM-MDSCs were cultured with or without 40% TES, 1 mM L-NAC (Sigma-Aldrich), 100 µM L-NMMA (Cayman Chemical), or 100 µM nor-NOHA (Cayman Chemical). TES was produced by culturing B16F10 tumor cells, freshly prepared from B16F10 tumors, at 1 × 10^7 tumor cells/ml for 24 h, and stored at −80°C until use.

Immunoblot

The cells were lysed in radioimmunoprecipitation assay buffer (Beyotime) in the presence of protease inhibitors (Roche). Whole-cell lysates were prepared and subjected to 10% SDS-PAGE (GeneStar) and transferred to polyvinylidene fluoride membrane (Bio-Rad). The membranes were probed overnight at 4°C with the antibodies specific for TIPE2 (Proteintech), ARG1, iNOS, p-STAT3 (Tyr705), STAT3, p-ERK (p-Erk1/2, Thr202/Tyr204), ERK (Erk1/2), p-AKT (Ser473), AKT, p-GSK-3β (Ser9), GSK-3β, p-C/EBPβ (Thr235, Thr188, and Thr47), p-threonine (Cell Signaling Technology), p47^{phox}, C/EBPβ, and β-actin (Santa Cruz), at a 1:1,000 dilution (all antibodies shown in Table S2). Membranes were washed and incubated for 1 h at room temperature with secondary antibodies conjugated with peroxidase. Membrane-bound immune complexes were detected using Super ECL detection reagent (Applygen) on an Amersham Imager 600 (GE Healthcare).

Arginase enzymatic activity and NO production

Arginase activity was measured in cell lysates as previously described (Corzo et al., 2010). In brief, cells were lysed for 30 min with 0.1% Triton X-100. To 100 µl of protein lysate (25 µg/ml), 100 µl of 25 mM Tris-HCl and 10 µl of 10 mM $MnCl_2$ were added, and the enzyme was activated by heating for 10 min at 56°C. Arginine hydrolysis was conducted by incubating the lysate with 100 µl of 0.5 M L-arginine, pH 9.7, at 37°C for 120 min. The reaction was stopped with 900 µl H_2SO_4 (96%)/H_3PO_4 (85%)/H_2O (1:3:7, vol:vol:vol). The urea concentration was measured at 540 nm after addition of 40 µl β-isonitrosopropiophenone (dissolved in 100% ethanol; Sigma-Aldrich), followed by heating at 95°C for 30 min. One unit of enzyme activity is defined as the amount of enzyme that catalyzed the formation of 1 µmol urea per min.

To detect NO production, equal volumes of cell culture supernatants (100 µl) were mixed with Greiss reagent (Beyotime). After a 10-min incubation at room temperature, the absorbance at 550 nm was measured using a microplate plate reader (Thermo NanoDrop 2000c). NO concentrations were determined by comparing the absorbance values for the test samples to a standard curve generated by serial dilution of 0.25 mM sodium nitrite.

ELISA

ELISA was used to determine the concentrations of IL-6, IL-10, TGF-β1, TNF-α, and IL-12 in the lysates or culture supernatants of MDSCs.

Lentivirus-mediated gene silencing or overexpressing assays

For silencing assays, HEK293T cells (ATCC) were transfected with mouse *Tipe2* siRNA, mouse *p47^{phox}* shRNA, human *Tipe2* shRNA, and scrambled control siRNA or shRNA plasmids (all sequences shown in Table S1) with pLKO.1-TRC lentiviral packaging constructs (Addgene) using Lipofectamine 3000 (Life Technology), according to the manufacturer's instructions. The virus supernatants were harvested 48 h after transfection, filtered, concentrated by ultracentrifugation, and titrated by limiting dilution assay using HEK293T cells. BM-MDSCs were infected by mouse *Tipe2* siRNA or mouse *p47^{phox}* shRNA lentivirus for 48 h, and cells were collected to measure TIPE2 and p47^{phox} knockdown efficiency by immunoblotting. MDSCs from PBMC cultures were infected with human *Tipe2* shRNA lentivirus for 48 h, and cells were collected to measure human TIPE2 knockdown efficiency by immunoblotting. For overexpressing assays, HEK293T cells (ATCC) were transfected with mouse LAP, mouse LIP, and control vector plasmids (all sequences shown in Table S1) with pLVX-IRES-ZsGreen1 lentiviral packaging constructs (Clontech, Takara) for 48 h, and cells were collected to measure LAP or LIP overexpression efficiency by immunoblotting.

ChIP assays

ChIP assays were performed using SimpleChip kits (Cell Signaling Technology). Chromatin was prepared from 4 × 10^6 MDSCs positively selected from spleens of WT and *Tipe2*$^{-/-}$ mice bearing B16F10 tumors. Chromatin was immunoprecipitated with antibodies against C/EBPβ, histone H3, or rabbit control IgG. Eluted and purified DNA was analyzed by qPCR with prevalidated primers (shown in Table S1 and synthesized by Synbio Technologies) against the IL-6 promoter (C/EBPβ) and the IL-10 promoter (C/EBPβ).

Immunoprecipitation

Lysates from 12 × 10^6 splenic MDSCs of WT and *Tipe2*$^{-/-}$ mice bearing B16F10 tumors were incubated overnight with 10 µg of antibodies against C/EBPβ at 4°C. The pulled-down proteins on protein G agarose beads (Cell Signaling Technology) were separated by centrifugation, washed several times with 0.5% PBST, and boiled with sample buffer for 5 min at 100°C, followed by centrifugation to collect supernatant and immunoblotting using

antibodies for p-C/EBPβ (Thr235), p-threonine (Cell Signaling Technology), and C/EBPβ.

H&E staining and IHC

B16F10 tumors were fixed in 10% neutral buffered formalin, embedded in paraffin, sectioned, and stained with H&E (Sigma-Aldrich) and/or cleaved caspase 3 antibody (Cell Signaling Technology).

mIHC and imaging analysis

We purchased the lung cancer tissue array (HLugA180Su03) from Shanghai Outdo Biotech and performed mIHC using an Opal 7-color fluorescent IHC kit (PerkinElmer) combined with automated quantitative analysis (AQUA; Genoptix) to assess the expression of HLA-DR, CD33, CD11b, CD14, CD66b, and TIPE2. First, the concentration and the order of the seven antibodies were optimized, and the spectral library was built based on the single-stained slides. Slides were dewaxed and rehydrated through a series of xylene-to-alcohol washes before being incubated in distilled water. mIHC staining was then performed after heat-induced antigen retrieval. Primary antibodies to the following antigens were used: HLA-DR (1:100; Abcam), CD33 (1:500; Abcam), CD11b (1:500; Proteintech), CD14 (1:100; Cell Signaling Technology), CD66b (1:500; Abcam), and TIPE2 (1:100; Proteintech). The following secondary antibodies were used: anti-mouse Envision HRP (Dako), anti-rabbit Envision HRP (Dako) and DAPI. Fluorescence images were acquired using the Vectra 2 Intelligent Slide Analysis System using Vectra software v2.0.8 (PerkinElmer).

First, monochrome imaging of the slide at 4× magnification using DAPI was conducted. An automated algorithm (developed using inForm software) was used to identify areas of the slide containing tissue to create RGB (red-green-blue) images. Accepted images were processed using AQUAduct (PerkinElmer), wherein each fluorophore was spectrally unmixed into individual channels and saved as a separate file. These files were analyzed using AQUAnalysis software. DAPI was used to generate a binary mask of all viable cells in the image. Similarly, HLA-DR, CD33, CD11b, CD14, CD66b, and TIPE2 expression was used in conjunction with DAPI to create binary masks of all cells expressing these biomarkers of interest. Additionally, the binary mask of CD14 or CD66b was further combined with the CD33 and CD11b double-positive masks to limit the analysis to M-MDSCs or G-MDSCs. The total area of M-MDSCs or G-MDSCs, measured in pixels, was divided by the total area of the $CD33^+CD11b^+$ cells, measured in pixels, to determine the percentage of M-MDSCs or G-MDSCs, respectively. Next, the binary mask of TIPE2 was combined with $CD14^+CD33^+CD11b^+$ or $CD66b^+CD33^+CD11b^+$ masks to determine the high (with >15% cells positive for TIPE2) or low (1–15% cells positive for TIPE2) expression of TIPE2.

RNA-seq and gene set enrichment analysis (GSEA)

$CD45^+CD11b^+Gr\text{-}1^+$ MDSCs from tumors of WT and *Tipe2*$^{-/-}$ C57BL/6 mice (6–8 wk old) were enriched with CD45 beads and sorted on a FACSAria III (BD Bioscience). The purity of MDSCs was >95%. RNA-seq was performed on the BGISEQ500 platform (BGI-Shenzhen). RNA-seq data were aligned using bowtie2 against mm10 version of the mouse genome, and RSEM v1.2.12 software was used to estimate the raw read counts using Ensemble v84 gene information. DESeq2 was used to estimate the significance of differential expression between sample groups. Overall gene expression changes were considered significant if their false discovery rate was <5%. RNA-seq data have been deposited in the Sequence Read Archive database (accession no. PRJNA545000). For tumor MDSC data, differentially expressed genes were identified as those that satisfy both Student's *t* test nominal P value of <0.05 and have a mean log2 expression difference of ≥1. For the analysis of M1 signatures, GSEA was performed using the Broad Institute's GSEA program. M1 Signature was copied from M1 gene set reported by Pan et al. (2017).

qPCR

Total RNA was isolated from MDSCs using TRIzol (Takara). RNA was then converted to cDNA using PrimeScript RT Master Mix (Takara). qPCR was performed on a Bio-Rad Thermal Cycler (S1000) using SYBR Premix Ex Taq II (Takara) with primers against indicated murine genes. Relative expression was calculated using the delta-delta Ct method and normalized to the reference gene *β-actin*. All primers were synthesized by Invitrogen and are shown in Table S1.

Statistical analyses

Statistical analyses were performed using Prism 6 software (GraphPad). All data are presented as mean ± SEM, and $P < 0.05$ was considered significant. The repeated measurements of tumor growth were assessed by two-way ANOVA. Kaplan–Meier survival analysis was performed for the comparison of survival curves. In figures, asterisks were used as follows: *, $P \le 0.05$; **, $P \le 0.01$; ***, $P \le 0.001$; and ****, $P \le 0.0001$.

Online supplemental material

Fig. S1 shows the impact of TIPE2 deletion on tumor growth, necrosis, and metastasis and spleen size. Fig. S2 shows flow cytometry analyses of leukocytes and the effect of anti-Gr-1 treatment in mice. Fig. S3 shows the impact of TIPE2 deletion on MDSC precursor differentiation, MDSC apoptosis, and function. Fig. S4 shows the impact of TIPE2 deletion on gene expression and protein expression profiles in tumor-infiltrating MDSCs. Fig. S5 shows that lung cancer patients with high-TIPE2 MDSCs had poor long-term survival and TIPE2 control of MDSCs and T cell–dependent responses to cancer. Table S1 shows primers used for PCR or sequences used for plasmid construction. Table S2 shows key resources including antibodies, reagents, plasmids, and mice. Table S3 shows genes of the heatmap in Fig. S4 A.

Acknowledgments

We thank members of the Public Technology Service Cores at the Shenzhen Institutes of Advanced Technology, Chinese Academy of Sciences, for their technical assistance.

This work was supported by the National Natural Science Foundation of China (grants 81501356 and 81373112), the

Science and Technology Project of Guangdong (grant 2013B01 0404038), the Shenzhen Basic Science Research Project (grants JCYJ20160229201353324, JCYJ20170413153158716, and JCYJ201 70818164619194), the Shenzhen Technology Innovation Project (grant JSGG20160229202150023), Nanshan Pilot Team Project (grant LHTD20160004), the Shenzhen Peacock Next-Generation Monoclonal Antibody Drug Research and Development Program (grant 1110140040347265), the Fourth Talents Project of Guangdong Province (2014-1), the Special Funds for Major Science and Technology of Guangdong Province (grant 2013A022100037), Guangdong Provincial Research Award for Scholars, the Shenzhen Laboratory of Fully Human Antibody Engineering (Development and Reform Commission in Shenzhen [2014] grant 1782), and Shenzhen Special Funds for Industry of the Future (Development and Reform Commission in Shenzhen [2015] grant 971).

The authors declare no competing financial interests.

Author contributions: D. Yan and Y.H. Chen conceived the study and prepared the manuscript. X. Wan supervised the study and contributed to manuscript preparation. D. Yan carried out most of the experiments and statistical analyses. J. Wang helped with mouse tumor models and performed certain experiments. H. Sun and Q. Ruan provided the TIPE2-deficient mouse breeders. H. Zhang helped with lentivirus production. X. Yang and A. Zamani provided valuable discussions about experimental design. W. Chen and A. Tang provided lung cancer samples.

Submitted: 24 October 2018
Revised: 13 June 2019
Accepted: 1 October 2019

References

Agudo, J., and B.D. Brown. 2016. Silence of the ROS. *Immunity*. 44:520–522. https://doi.org/10.1016/j.immuni.2016.02.027

Bronte, V., S. Brandau, S.H. Chen, M.P. Colombo, A.B. Frey, T.F. Greten, S. Mandruzzato, P.J. Murray, A. Ochoa, S. Ostrand-Rosenberg, et al. 2016. Recommendations for myeloid-derived suppressor cell nomenclature and characterization standards. *Nat. Commun.* 7:12150. https://doi.org/10.1038/ncomms12150

Cancer Genome Atlas Research Network. 2014. Comprehensive molecular profiling of lung adenocarcinoma. *Nature*. 511:543–550. https://doi.org/10.1038/nature13385

Cheng, P., C.A. Corzo, N. Luetteke, B. Yu, S. Nagaraj, M.M. Bui, M. Ortiz, W. Nacken, C. Sorg, T. Vogl, et al. 2008. Inhibition of dendritic cell differentiation and accumulation of myeloid-derived suppressor cells in cancer is regulated by S100A9 protein. *J. Exp. Med.* 205:2235–2249. https://doi.org/10.1084/jem.20080132

Condamine, T., J. Mastio, and D.I. Gabrilovich. 2015. Transcriptional regulation of myeloid-derived suppressor cells. *J. Leukoc. Biol.* 98:913–922. https://doi.org/10.1189/jlb.4RI0515-204R

Corzo, C.A., T. Condamine, L. Lu, M.J. Cotter, J.I. Youn, P. Cheng, H.I. Cho, E. Celis, D.G. Quiceno, T. Padhya, et al. 2010. HIF-1α regulates function and differentiation of myeloid-derived suppressor cells in the tumor microenvironment. *J. Exp. Med.* 207:2439–2453. https://doi.org/10.1084/jem.20100587

Corzo, C.A., M.J. Cotter, P. Cheng, F. Cheng, S. Kusmartsev, E. Sotomayor, T. Padhya, T.V. McCaffrey, J.C. McCaffrey, and D.I. Gabrilovich. 2009. Mechanism regulating reactive oxygen species in tumor-induced myeloid-derived suppressor cells. *J. Immunol.* 182:5693–5701. https://doi.org/10.4049/jimmunol.0900092

Fan, Y.C., N. Wang, Y.Y. Sun, X.Y. Xiao, and K. Wang. 2015. TIPE2 mRNA Level in PBMCs Serves as a Novel Biomarker for Predicting Short-Term Mortality of Acute-on-Chronic Hepatitis B Liver Failure: A Prospective Single-Center Study. *Medicine (Baltimore)*. 94:e1638. https://doi.org/10.1097/MD.0000000000001638

Fayngerts, S.A., Z. Wang, A. Zamani, H. Sun, A.E. Boggs, T.P. Porturas, W. Xie, M. Lin, T. Cathopoulis, J.R. Goldsmith, et al. 2017. Direction of leukocyte polarization and migration by the phosphoinositide-transfer protein TIPE2. *Nat. Immunol.* 18:1353–1360. https://doi.org/10.1038/ni.3866

Gabrilovich, D.I. 2017. Myeloid-Derived Suppressor Cells. *Cancer Immunol. Res.* 5:3–8. https://doi.org/10.1158/2326-6066.CIR-16-0297

Gus-Brautbar, Y., D. Johnson, L. Zhang, H. Sun, P. Wang, S. Zhang, L. Zhang, and Y.H. Chen. 2012. The anti-inflammatory TIPE2 is an inhibitor of the oncogenic Ras. *Mol. Cell.* 45:610–618. https://doi.org/10.1016/j.molcel.2012.01.006

He, Y.M., X. Li, M. Perego, Y. Nefedova, A.V. Kossenkov, E.A. Jensen, V. Kagan, Y.F. Liu, S.Y. Fu, Q.J. Ye, et al. 2018. Transitory presence of myeloid-derived suppressor cells in neonates is critical for control of inflammation. *Nat. Med.* 24:224–231. https://doi.org/10.1038/nm.4467

Hirai, H., P. Zhang, T. Dayaram, C.J. Hetherington, S. Mizuno, J. Imanishi, K. Akashi, and D.G. Tenen. 2006. C/EBPbeta is required for 'emergency' granulopoiesis. *Nat. Immunol.* 7:732–739. https://doi.org/10.1038/ni1354

Kumar, V., P. Cheng, T. Condamine, S. Mony, L.R. Languino, J.C. McCaffrey, N. Hockstein, M. Guarino, G. Masters, E. Penman, et al. 2016a. CD45 Phosphatase Inhibits STAT3 Transcription Factor Activity in Myeloid Cells and Promotes Tumor-Associated Macrophage Differentiation. *Immunity*. 44:303–315. https://doi.org/10.1016/j.immuni.2016.01.014

Kumar, V., S. Patel, E. Tcyganov, and D.I. Gabrilovich. 2016b. The Nature of Myeloid-Derived Suppressor Cells in the Tumor Microenvironment. *Trends Immunol.* 37:208–220. https://doi.org/10.1016/j.it.2016.01.004

Leavy, O. 2014. Inflammation: Regulating ROS. *Nat. Rev. Immunol.* 14:357. https://doi.org/10.1038/nri3685

Lee, C.K., R. Raz, R. Gimeno, R. Gertner, B. Wistinghausen, K. Takeshita, R.A. DePinho, and D.E. Levy. 2002. STAT3 is a negative regulator of granulopoiesis but is not required for G-CSF-dependent differentiation. *Immunity*. 17:63–72. https://doi.org/10.1016/S1074-7613(02)00336-9

Li, F., X. Zhu, Y. Yang, L. Huang, and J. Xu. 2016. TIPE2 Alleviates Systemic Lupus Erythematosus Through Regulating Macrophage Polarization. *Cell. Physiol. Biochem.* 38:330–339. https://doi.org/10.1159/000438633

Li, Y., E. Bevilacqua, C.B. Chiribau, M. Majumder, C. Wang, C.M. Croniger, M.D. Snider, P.F. Johnson, and M. Hatzoglou. 2008. Differential control of the CCAAT/enhancer-binding protein beta (C/EBPbeta) products liver-enriched transcriptional activating protein (LAP) and liver-enriched transcriptional inhibitory protein (LIP) and the regulation of gene expression during the response to endoplasmic reticulum stress. *J. Biol. Chem.* 283:22443–22456. https://doi.org/10.1074/jbc.M801046200

Lou, Y., S. Liu, C. Zhang, G. Zhang, J. Li, M. Ni, G. An, M. Dong, X. Liu, F. Zhu, et al. 2013. Enhanced atherosclerosis in TIPE2-deficient mice is associated with increased macrophage responses to oxidized low-density lipoprotein. *J. Immunol.* 191:4849–4857. https://doi.org/10.4049/jimmunol.1300053

Lou, Y., H. Sun, S. Morrissey, T. Porturas, S. Liu, X. Hua, and Y.H.H. Chen. 2014. Critical roles of TIPE2 protein in murine experimental colitis. *J. Immunol.* 193:1064–1070. https://doi.org/10.4049/jimmunol.1400415

Lu, Q., Z. Liu, Z. Li, J. Chen, Z. Liao, W.R. Wu, and Y.W. Li. 2016. TIPE2 Overexpression Suppresses the Proliferation, Migration, and Invasion in Prostate Cancer Cells by Inhibiting PI3K/Akt Signaling Pathway. *Oncol. Res.* 24:305–313. https://doi.org/10.3727/096504016X14666990347437

Maekawa, T., K. Hosur, T. Abe, A. Kantarci, A. Ziogas, B. Wang, T.E. Van Dyke, T. Chavakis, and G. Hajishengallis. 2015. Antagonistic effects of IL-17 and D-resolvins on endothelial Del-1 expression through a GSK-3β-C/EBPβ pathway. *Nat. Commun.* 6:8272. https://doi.org/10.1038/ncomms9272

Manderson, A.P., J.G. Kay, L.A. Hammond, D.L. Brown, and J.L. Stow. 2007. Subcompartments of the macrophage recycling endosome direct the differential secretion of IL-6 and TNFalpha. *J. Cell Biol.* 178:57–69. https://doi.org/10.1083/jcb.200612131

Manjili, M.H. 2012. Phenotypic plasticity of MDSC in cancers. *Immunol. Invest.* 41:711–721. https://doi.org/10.3109/08820139.2012.673670

Marigo, I., E. Bosio, S. Solito, C. Mesa, A. Fernandez, L. Dolcetti, S. Ugel, N. Sonda, S. Bicciato, E. Falisi, et al. 2010. Tumor-induced tolerance and immune suppression depend on the C/EBPbeta transcription factor. *Immunity*. 32:790–802. https://doi.org/10.1016/j.immuni.2010.05.010

Marigo, I., L. Dolcetti, P. Serafini, P. Zanovello, and V. Bronte. 2008. Tumor-induced tolerance and immune suppression by myeloid derived suppressor cells. *Immunol. Rev.* 222:162–179. https://doi.org/10.1111/j.1600-065X.2008.00602.x

Mildner, A., J. Schönheit, A. Giladi, E. David, D. Lara-Astiaso, E. Lorenzo-Vivas, F. Paul, L. Chappell-Maor, J. Priller, A. Leutz, et al. 2017. Genomic Characterization of Murine Monocytes Reveals C/EBPβ Transcription Factor Dependence of Ly6C$^-$ Cells. *Immunity*. 46:849–862.e7. https://doi.org/10.1016/j.immuni.2017.04.018

Mundy-Bosse, B.L., G.B. Lesinski, A.C. Jaime-Ramirez, K. Benninger, M. Khan, P. Kuppusamy, K. Guenterberg, S.V. Kondadasula, A.R. Chaudhury, K.M. La Perle, et al. 2011. Myeloid-derived suppressor cell inhibition of the IFN response in tumor-bearing mice. *Cancer Res.* 71: 5101–5110. https://doi.org/10.1158/0008-5472.CAN-10-2670

Nathan, C., and A. Cunningham-Bussel. 2013. Beyond oxidative stress: an immunologist's guide to reactive oxygen species. *Nat. Rev. Immunol.* 13: 349–361. https://doi.org/10.1038/nri3423

Ostrand-Rosenberg, S. 2010. Myeloid-derived suppressor cells: more mechanisms for inhibiting antitumor immunity. *Cancer Immunol. Immunother.* 59:1593–1600. https://doi.org/10.1007/s00262-010-0855-8

Pan, W., S. Zhu, K. Qu, K. Meeth, J. Cheng, K. He, H. Ma, Y. Liao, X. Wen, C. Roden, et al. 2017. The DNA Methylcytosine Dioxygenase Tet2 Sustains Immunosuppressive Function of Tumor-Infiltrating Myeloid Cells to Promote Melanoma Progression. *Immunity.* 47:284–297.e5. https://doi.org/10.1016/j.immuni.2017.07.020

Panopoulos, A.D., L. Zhang, J.W. Snow, D.M. Jones, A.M. Smith, K.C. El Kasmi, F. Liu, M.A. Goldsmith, D.C. Link, P.J. Murray, and S.S. Watowich. 2006. STAT3 governs distinct pathways in emergency granulopoiesis and mature neutrophils. *Blood.* 108:3682–3690. https://doi.org/10.1182/blood-2006-02-003012

Park, B.H., S. Kook, S. Lee, J.H. Jeong, A. Brufsky, and B.C. Lee. 2013. An isoform of C/EBPβ, LIP, regulates expression of the chemokine receptor CXCR4 and modulates breast cancer cell migration. *J. Biol. Chem.* 288: 28656–28667. https://doi.org/10.1074/jbc.M113.509505

Qin, A., W. Cai, T. Pan, K. Wu, Q. Yang, N. Wang, Y. Liu, D. Yan, F. Hu, P. Guo, et al. 2013. Expansion of monocytic myeloid-derived suppressor cells dampens T cell function in HIV-1-seropositive individuals. *J. Virol.* 87: 1477–1490. https://doi.org/10.1128/JVI.01759-12

Quatromoni, J.G., S. Singhal, P. Bhojnagarwala, W.W. Hancock, S.M. Albelda, and E. Eruslanov. 2015. An optimized disaggregation method for human lung tumors that preserves the phenotype and function of the immune cells. *J. Leukoc. Biol.* 97:201–209. https://doi.org/10.1189/jlb.5TA0814-373

Rehm, A., M. Gätjen, K. Gerlach, F. Scholz, A. Mensen, M. Gloger, K. Heinig, B. Lamprecht, S. Mathas, V. Bégay, et al. 2014. Dendritic cell-mediated survival signals in Eμ-Myc B-cell lymphoma depend on the transcription factor C/EBPβ. *Nat. Commun.* 5:5057. https://doi.org/10.1038/ncomms6057

Ruffell, D., F. Mourkioti, A. Gambardella, P. Kirstetter, R.G. Lopez, N. Rosenthal, and C. Nerlov. 2009. A CREB-C/EBPbeta cascade induces M2 macrophage-specific gene expression and promotes muscle injury repair. *Proc. Natl. Acad. Sci. USA.* 106:17475–17480. https://doi.org/10.1073/pnas.0908641106

Shen, F., N. Li, P. Gade, D.V. Kalvakolanu, T. Weibley, B. Doble, J.R. Woodgett, T.D. Wood, and S.L. Gaffen. 2009. IL-17 receptor signaling inhibits C/EBPbeta by sequential phosphorylation of the regulatory 2 domain. *Sci. Signal.* 2:ra8. https://doi.org/10.1126/scisignal.2000066

Solito, S., L. Pinton, V. Damuzzo, and S. Mandruzzato. 2012. Highlights on molecular mechanisms of MDSC-mediated immune suppression: paving the way for new working hypotheses. *Immunol. Invest.* 41:722–737. https://doi.org/10.3109/08820139.2012.678023

Sonda, N., F. Simonato, E. Peranzoni, B. Calì, S. Bortoluzzi, A. Bisognin, E. Wang, F.M. Marincola, L. Naldini, B. Gentner, et al. 2013. miR-142-3p prevents macrophage differentiation during cancer-induced myelopoiesis. *Immunity.* 38:1236–1249. https://doi.org/10.1016/j.immuni.2013.06.004

Srivastava, M.K., L. Zhu, M. Harris-White, U.K. Kar, M. Huang, M.F. Johnson, J.M. Lee, D. Elashoff, R. Strieter, S. Dubinett, and S. Sharma. 2012. Myeloid suppressor cell depletion augments antitumor activity in lung cancer. *PLoS One.* 7:e40677. https://doi.org/10.1371/journal.pone.0040677

Stromnes, I.M., J.S. Brockenbrough, K. Izeradjene, M.A. Carlson, C. Cuevas, R.M. Simmons, P.D. Greenberg, and S.R. Hingorani. 2014. Targeted depletion of an MDSC subset unmasks pancreatic ductal adenocarcinoma to adaptive immunity. *Gut.* 63:1769–1781. https://doi.org/10.1136/gutjnl-2013-306271

Sun, H., S. Gong, R.J. Carmody, A. Hilliard, L. Li, J. Sun, L. Kong, L. Xu, B. Hilliard, S. Hu, et al. 2008. TIPE2, a negative regulator of innate and adaptive immunity that maintains immune homeostasis. *Cell.* 133: 415–426. https://doi.org/10.1016/j.cell.2008.03.026

Sun, H., G. Zhuang, L. Chai, Z. Wang, D. Johnson, Y. Ma, and Y.H.H. Chen. 2012. TIPE2 controls innate immunity to RNA by targeting the phosphatidylinositol 3-kinase-Rac pathway. *J. Immunol.* 189:2768–2773. https://doi.org/10.4049/jimmunol.1103477

Suo, L.G., Y.Y. Cui, Y. Bai, and X.J. Qin. 2016. Anti-inflammatory TIPE2 inhibits angiogenic VEGF in retinal pigment epithelium. *Mol. Immunol.* 73: 46–52. https://doi.org/10.1016/j.molimm.2016.03.013

Tamura, A., H. Hirai, A. Yokota, N. Kamio, A. Sato, T. Shoji, T. Kashiwagi, Y. Torikoshi, Y. Miura, D.G. Tenen, and T. Maekawa. 2017. C/EBPβ is required for survival of Ly6C$^-$ monocytes. *Blood.* 130:1809–1818. https://doi.org/10.1182/blood-2017-03-772962

Thevenot, P.T., R.A. Sierra, P.L. Raber, A.A. Al-Khami, J. Trillo-Tinoco, P. Zarreii, A.C. Ochoa, Y. Cui, L. Del Valle, and P.C. Rodriguez. 2014. The stress-response sensor chop regulates the function and accumulation of myeloid-derived suppressor cells in tumors. *Immunity.* 41:389–401. https://doi.org/10.1016/j.immuni.2014.08.015

Trikha, P., and W.E. Carson III. 2014. Signaling pathways involved in MDSC regulation. *Biochim. Biophys. Acta.* 1846:55–65.

Tschopp, J., and K. Schroder. 2010. NLRP3 inflammasome activation: The convergence of multiple signalling pathways on ROS production? *Nat. Rev. Immunol.* 10:210–215. https://doi.org/10.1038/nri2725

Tsukagoshi, H., W. Busch, and P.N. Benfey. 2010. Transcriptional regulation of ROS controls transition from proliferation to differentiation in the root. *Cell.* 143:606–616. https://doi.org/10.1016/j.cell.2010.10.020

Veglia, F., M. Perego, and D. Gabrilovich. 2018. Myeloid-derived suppressor cells coming of age. *Nat. Immunol.* 19:108–119. https://doi.org/10.1038/s41590-017-0022-x

Veglia, F., V.A. Tyurin, M. Blasi, A. De Leo, A.V. Kossenkov, L. Donthireddy, T.K.J. To, Z. Schug, S. Basu, F. Wang, et al. 2019. Fatty acid transport protein 2 reprograms neutrophils in cancer. *Nature.* 569:73–78. https://doi.org/10.1038/s41586-019-1118-2

Wang, K., Y. Ren, Y. Liu, J. Zhang, and J.J. He. 2017. Tumor Necrosis Factor (TNF)-α-Induced Protein 8-like-2 (TIPE2) Inhibits Proliferation and Tumorigenesis in Breast Cancer Cells. *Oncol. Res.* 25:55–63. https://doi.org/10.3727/096504016X14719078133320

Wang, Z., S. Fayngerts, P. Wang, H. Sun, D.S. Johnson, Q. Ruan, W. Guo, and Y.H.H. Chen. 2012. TIPE2 protein serves as a negative regulator of phagocytosis and oxidative burst during infection. *Proc. Natl. Acad. Sci. USA.* 109:15413–15418. https://doi.org/10.1073/pnas.1204525109

Wu, J., H. Zhang, C. Xu, H. Xu, X. Zhou, Y. Xie, and M. Tao. 2016. TIPE2 functions as a metastasis suppressor via negatively regulating β-catenin through activating GSK3β in gastric cancer. *Int. J. Oncol.* 48:199–206. https://doi.org/10.3892/ijo.2015.3224

Yan, D., A.O. Adeshakin, M. Xu, L.O. Afolabi, G. Zhang, Y.H. Chen, and X. Wan. 2019. Lipid Metabolic Pathways Confer the Immunosuppressive Function of Myeloid-Derived Suppressor Cells in Tumor. *Front. Immunol.* 10:1399. https://doi.org/10.3389/fimmu.2019.01399

Yan, D., Q. Yang, M. Shi, L. Zhong, C. Wu, T. Meng, H. Yin, and J. Zhou. 2013. Polyunsaturated fatty acids promote the expansion of myeloid-derived suppressor cells by activating the JAK/STAT3 pathway. *Eur. J. Immunol.* 43:2943–2955. https://doi.org/10.1002/eji.201343472

Yan, D.H., J.H. Wang, and X.C. Wan. 2017. TIPE2 is a novel direct target of STAT3 in MDSC and inhibition of its expression on MDSC enhanced T cell activation in tumor. *J. Immunol.* 198:205.3.

Yang, Q., J. Wei, L. Zhong, M. Shi, P. Zhou, S. Zuo, K. Wu, M. Zhu, X. Huang, Y. Yu, et al. 2015. Cross talk between histone deacetylase 4 and STAT6 in the transcriptional regulation of arginase 1 during mouse dendritic cell differentiation. *Mol. Cell. Biol.* 35:63–75. https://doi.org/10.1128/MCB.00805-14

Zhang, H., H. Nguyen-Jackson, A.D. Panopoulos, H.S. Li, P.J. Murray, and S.S. Watowich. 2010a. STAT3 controls myeloid progenitor growth during emergency granulopoiesis. *Blood.* 116:2462–2471. https://doi.org/10.1182/blood-2009-12-259630

Zhang, S., Y. Zhang, X. Wei, J. Zhen, Z. Wang, M. Li, W. Miao, H. Ding, P. Du, W. Zhang, et al. 2010b. Expression and regulation of a novel identified TNFAIP8 family is associated with diabetic nephropathy. *Biochim. Biophys. Acta.* 1802:1078–1086. https://doi.org/10.1016/j.bbadis.2010.08.003

Zhang, X., J. Wang, C. Fan, H. Li, H. Sun, S. Gong, Y.H.H. Chen, and Y. Shi. 2009. Crystal structure of TIPE2 provides insights into immune homeostasis. *Nat. Struct. Mol. Biol.* 16:89–90. https://doi.org/10.1038/nsmb.1522

Zhang, Y., X. Wei, L. Liu, S. Liu, Z. Wang, B. Zhang, B. Fan, F. Yang, S. Huang, F. Jiang, et al. 2012. TIPE2, a novel regulator of immunity, protects against experimental stroke. *J. Biol. Chem.* 287:32546–32555. https://doi.org/10.1074/jbc.M112.348755

Zhou, J., Y. Nefedova, A. Lei, and D. Gabrilovich. 2018. Neutrophils and PMN-MDSC: Their biological role and interaction with stromal cells. *Semin. Immunol.* 35:19–28. https://doi.org/10.1016/j.smim.2017.12.004